AGU PUBLICATIONS

JGR

Journal of Geophysical Research: Solid Earth

RESEARCH ARTICLE
10.1002/2015JB011970

Key Points:
- Laboratory study on the influence of talc on the frictional behavior of calcite
- Addition of talc strongly weakens calcite gouges and favors stable sliding
- Mechanical behavior results from a change in deformation mechanisms

Supporting Information:
- Figures S1–S5 and Table S1

Correspondence to:
C. Giorgetti,
carolina.giorgetti@uniroma1.it

Citation:
Giorgetti, C., B. M. Carpenter, and C. Collettini (2015), Frictional behavior of talc-calcite mixtures, *J. Geophys. Res. Solid Earth*, *120*, doi:10.1002/2015JB011970.

Received 19 FEB 2015
Accepted 18 AUG 2015
Accepted article online 22 AUG 2015

Frictional behavior of talc-calcite mixtures

C. Giorgetti[1], B. M. Carpenter[2], and C. Collettini[1,2]

[1]Dipartimento di Scienze della Terra, Università degli Studi La Sapienza, Rome, Italy, [2]Istituto Nazionale di Geofisica e Vulcanologia, Rome, Italy

Abstract Faults involving phyllosilicates appear weak when compared to the laboratory-derived strength of most crustal rocks. Among phyllosilicates, talc, with very low friction, is one of the weakest minerals involved in various tectonic settings. As the presence of talc has been recently documented in carbonate faults, we performed laboratory friction experiments to better constrain how various amounts of talc could alter these fault's frictional properties. We used a biaxial apparatus to systematically shear different mixtures of talc and calcite as powdered gouge at room temperature, normal stresses up to 50 MPa and under different pore fluid saturated conditions, i.e., $CaCO_3$-equilibrated water and silicone oil. We performed slide-hold-slide tests, 1–3000 s, to measure the amount of frictional healing and velocity-stepping tests, 0.1–1000 μm/s, to evaluate frictional stability. We then analyzed microstructures developed during our experiments. Our results show that with the addition of 20% talc the calcite gouge undergoes a 70% reduction in steady state frictional strength, a complete reduction of frictional healing and a transition from velocity-weakening to velocity-strengthening behavior. Microstructural analysis shows that with increasing talc content, deformation mechanisms evolve from distributed cataclastic flow of the granular calcite to localized sliding along talc-rich shear planes, resulting in a fully interconnected network of talc lamellae from 20% talc onward. Our observations indicate that in faults where talc and calcite are present, a low concentration of talc is enough to strongly modify the gouge's frictional properties and specifically to weaken the fault, reduce its ability to sustain future stress drops, and stabilize slip.

1. Introduction

Geological studies show that mature fault zones can contain a variable amount of phyllosilicates [e.g., *Wintsch et al*., 1995; *Vrolijk and van der Pluijm*, 1999; *Faulkner et al*., 2003; *Collettini and Holdsworth*, 2004; *Jefferies et al*., 2006; *Fagereng and Sibson*, 2010]. Talc, in particular, has been documented in exhumed subduction thrust faults [e.g., *Peacock*, 1987; *Bebout and Barton*, 2002; *King et al*., 2003], in oceanic transform faults [*d'Orazio et al*., 2004], and in oceanic detachments [e.g., *Escartín et al*., 2003; *Schroeder and John*, 2004]. Drilling projects have reported the presence of talc within active traces of major faults at depth, such as the San Andreas fault in California [*Moore and Rymer*, 2007] and the Moresby fault in Papua New Guinea [e.g., *Floyd et al*., 2001; *Kopf*, 2001; *Roller et al*., 2001; *Taylor and Huchon*, 2002]. Talc has also been found along exhumed low-angle normal faults in Italy [*Collettini et al*., 2009b; *Viti and Collettini*, 2009] and in the Cyclades [*Grasemann and Tschegg*, 2012]. In subduction thrust faults, oceanic fracture zones, and oceanic detachments, talc is typically derived from the metamorphic alteration of ultramafic rocks with silica-saturated hydrothermal fluids [e.g., *Manning*, 1995; *Boschi et al*., 2006; *Moore and Rymer*, 2007]. In sedimentary rocks, talc development is the result of dissolution of dolomite and interaction with silica-rich fluids [*Collettini et al*., 2009b].

The presence of talc and other phyllosilicates within mature fault zones strongly influences the strength and slip behavior of those faults. Early laboratory experiments conducted on a vast gamut of rocks showed that friction was almost independent of rock type and is in the range of $\mu = 0.6$–0.85 [*Byerlee*, 1978]. Hereafter, we referred to rocks and faults whose coefficient of friction is within this range as strong, as opposed to rocks and faults whose coefficient of friction is half of or less than the values in this range, that are thus considered weak. The laboratory prediction of strong faults, with high friction, seems to be consistent with measurements of crustal stress levels in deep boreholes [*Townend and Zoback*, 2000] and the analysis of earthquake focal mechanisms [*Collettini and Sibson*, 2001]. However, in the last decade there is growing evidence for the presence of mechanically weak faults: including strike-slip faults, like the San Andreas [*Hickman and Zoback*, 2004; *Moore and Rymer*, 2007; *Schleicher et al*., 2010; *Carpenter et al*., 2011; *Lockner et al*., 2011], low-angle normal faults [*Numelin et al*., 2007; *Collettini et al*., 2009b] and thrust faults [*Kopf and Brown*, 2003; *Ikari et al*., 2009b; *Tesei et al*., 2014]. In all of these

structures, fault weakness is inferred to result from the development of through-going phyllosilicate-rich zones within the fault zone at the expense of the strong mineral phases. The importance of the distribution of weak and strong minerals in fault rocks has been further confirmed by laboratory experiments showing that intact, foliated samples are extremely weak when compared to powders derived from the same samples [e.g., *Collettini et al*., 2009a]. Phyllosilicates are characterized by a strong mechanical anisotropy, due their layered structure, that leads to the development of efficient planes of weakness, when the layers are favorably iso-oriented with respect to the shear.

Important questions for fault mechanics that remain are as follows: what percent of a weak mineral phase is capable of changing fault strength and how does the presence of weak mineral phases influence fault slip behavior? Experimental studies conducted on intact cores of slightly serpentinized peridotites have shown that small amounts of weak phase, i.e., 9% of lizardite and chrysotile, strongly affect the mechanical properties of peridotite, resulting in a mechanical behavior characteristic of pure serpentinites [*Escartín et al*., 2001]. Similarly, metasomatic growth of talc observed during shear experiments strongly weakens gouges, developing through-going shear surfaces [*Hirauchi et al*., 2013]. Previous experiments on mixtures of strong granular materials and weak platy minerals have highlighted the role of phyllosilicates in weakening granular fault gouges [e.g., *Bos and Spiers*, 2000; *Tembe et al*., 2010; *Moore and Lockner*, 2011]. For example, in quartz/montmorillonite mixtures, 50% of montmorillonite reduces friction, measured at about 9 mm of shear displacement, from 0.75 to 0.26 [*Tembe et al*., 2010]. In quartz/talc mixtures, 50% of talc is responsible for a friction drop, measured at about 3.5 mm of shear displacement, from 0.7 to 0.3 and promotes velocity-strengthening behavior, i.e., increasing friction with increasing velocity [*Moore and Lockner*, 2011]. The presence of weak platy minerals also reduces the ability of gouges to regain strength during nonshearing periods [*Niemeijer and Spiers*, 2006; *Carpenter et al*., 2011; *Tesei et al*., 2012].

In this manuscript we investigate the effect of increasing talc content on the frictional and healing properties of calcite by running experiments on binary mixtures of calcite and talc and looking at the microstructures developed within the experimental faults. Our study provides insights on fault slip behavior, not only for talc-rich faults developed within carbonates but also for those forming from serpentinites where calcite can be present along the fault zone due to hydrothermal cementation [e.g., *Bernoulli and Weissert*, 1985].

2. Experimental Method

2.1. Sample Description

Synthetic gouge mixtures used in this study were prepared from calcite and talc minerals in various proportions by weight. Calcite gouge was prepared from locally sourced Carrara Marble ($>$98% $CaCO_3$) that was crushed and sieved to $<$125 μm grain size (Figures S1 and S2 in the supporting information). Talc was prepared by separating talc grains from a talc-rich schist from Balmat, New York and was provided by Ward's Science. It was also crushed and sieved to $<$125 μm grain size (Figures S1 and S2).

We performed friction experiments in a servo-controlled biaxial testing apparatus installed in the High Pressure-High Temperature Laboratory at the Istituto Nazionale di Geofisica e Vulcanologia (INGV) in Rome, Italy [*Collettini et al*., 2014]. Stainless steel load cells continuously measure applied force with 0.03 kN resolution and linear variable differential transformer sensors continuously measure load point displacements with 0.1 μm resolution. Two layers of simulated fault gouge were placed in between three grooved sliding blocks, in a double-direct shear configuration [e.g., *Dieterich*, 1972; *Mair and Marone*, 1999; *Ikari et al*., 2011]. The two gouge layers, each with an initial ~5 mm uniform thickness measured before the samples were loaded, were constructed in order to have a 5 cm × 5 cm uniform area, that is maintained constant throughout the experiment (Figure 1a, inset).

2.2. Experimental Procedure

Experiments were performed at room temperature and under $CaCO_3$-equilibrated water-saturated conditions, except for two experiments, which were saturated with silicone oil. Initially, we ran a suite of 14 friction experiments under a constant normal stress of 5 MPa, in which talc content was systematically increased from 0% to 100%, in order to characterize the frictional behavior of the binary mixtures. Subsequently, we ran four more experiments under higher normal stress, i.e., 20 MPa and 50 MPa, focusing on 5% and 20% talc samples.

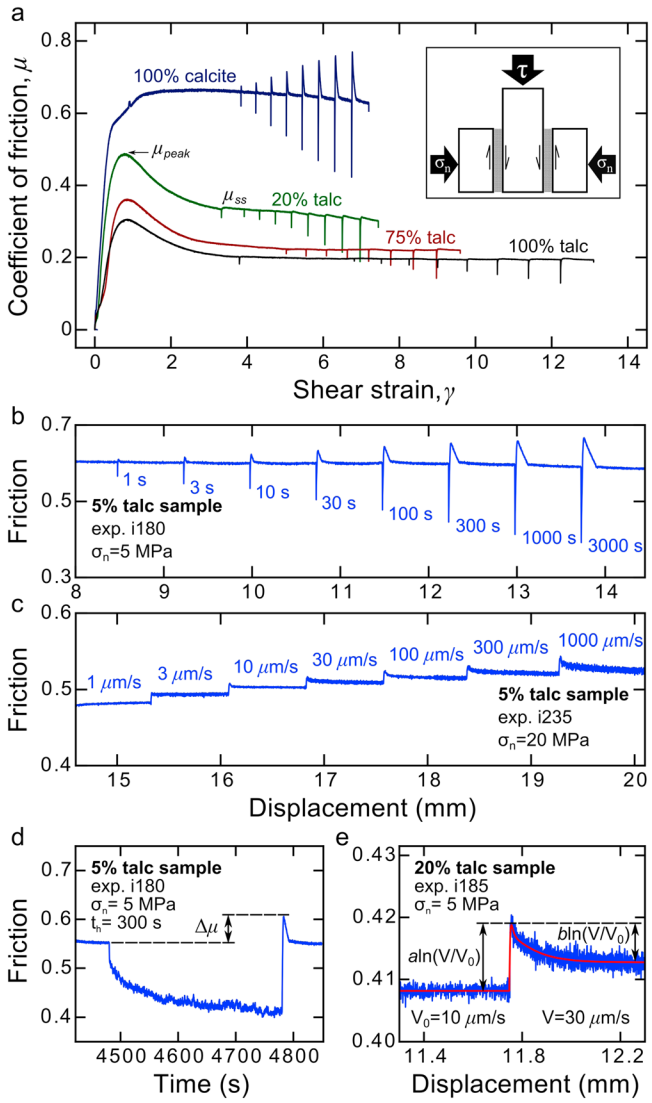

Figure 1. (a) Friction plotted against shear strain for selected slide-hold-slide friction experiments, showing the evolution of friction for different talc contents. During the "run-in" phase, peak friction is attained (μ_{peak}) and then evolves to a steady state value (μ_{ss}), as shown in the 20% talc sample. After the run-in, the slide-hold-slide and velocity step sequences are started. Inset shows the double-direct shear configuration in which three stainless steel forcing blocks sandwich two identical layers of experimental fault gouge. (b) Details of friction versus displacement for a slide-hold-slide sequence. (c) Details of friction versus displacement for a velocity step sequence. (d) Details of friction versus time for a 300 s hold. $\Delta\mu$ is the difference between the peak value of friction upon reshear and the prehold steady state friction. (e) Details of friction versus displacement for a 10–30 μm/s velocity step. The parameter *a* is proportional to the instantaneous change in friction and *b* is proportional to the subsequent drop to a new steady state. The red line shows the modeled output of the velocity step.

The experimental sample assembly was loaded into the testing apparatus and placed within a plastic membrane that was filled with the saturating fluid after the application of an initial normal load. Our experiments were performed under drained conditions. Initially we applied a normal stress of 1 MPa and allowed the sample to saturate for 30 min with deionized water that had been brought into equilibrium with $CaCO_3$. Layer compaction was monitored, checking after 30 min the achievement of a steady state value of layer thickness, that depends on the amount of compaction each gouge undergoes. Subsequently, normal stress was increased to the target value, i.e., 5, 20, or 50 MPa, and the sample was subjected to a shear displacement "run-in" of ~7.5–8.5 mm by imposing a load velocity of 10 μm/s to the vertical piston. The "run-in" phase allows for the development of a steady state friction (Figure 1a). Following steady shear, we imposed a series of computer-controlled changes in sliding velocity to test the time and velocity dependence of friction (Figure 1); we evaluated changes in friction in the context of rate- and state-dependent friction [e.g., *Marone*, 1998].

The coefficient of friction (μ) was calculated from the Coulomb criterion by dividing half of the vertical load (two gouge layers) by the horizontal load, i.e., the shear stress by the normal stress, and assuming no cohesion. The average shear strain within the layer was calculated by dividing shear displacement increments by the measured layer thickness and summing. The displacement values of the vertical and horizontal load points were corrected for the elastic stretch of each load frame, taking into account that the machine stiffness is 1283 kN/mm on the horizontal axis and 928.5 kN/mm on the vertical axis.

Following steady shear, we performed slide-hold-slide and velocity-stepping sequences (Table 1). Slide-hold-slide tests consist of a sequence of slide-hold-slide cycles: 75 s of sliding at 10 μm/s was followed by a hold period, t_h, ranging from 1 to 3000 s, during which sliding is halted and subsequently resumed (Figures 1a, 1b, and 1d), following the same procedure as in *Carpenter et al.* [2011] and *Tesei et al.* [2012]. The amount of frictional healing ($\Delta\mu$) is measured as the difference between the peak

Table 1. List of Experiments[a]

Experiment	Calcite/Talc (wt %)	σ_n (MPa)	Pore Fluid	Sequence of Hold Times (s)	Sequence of Velocity Steps (μm/s)
i040	100/0	5	$CaCO_3$-saturated water	1, 3, 10, 30, 100, 300, 1000, 3000	-
i180	95/5	5	$CaCO_3$-saturated water	1, 3, 10, 30, 100, 300, 1000, 3000	-
i179	90/10	5	$CaCO_3$-saturated water	1, 3, 10, 30, 100, 300, 1000, 3000	-
i176	80/20	5	$CaCO_3$-saturated water	1, 3, 10, 30, 100, 300, 1000, 3000	-
i175	70/30	5	$CaCO_3$-saturated water	1, 3, 10, 30, 100, 300, 1000, 3000	-
i174	60/40	5	$CaCO_3$-saturated water	1, 3, 10, 30, 100, 300, 1000, 3000	-
i050	50/50	5	$CaCO_3$-saturated water	1, 3, 10, 30, 100, 300, 1000, 3000	-
i181	25/75	5	$CaCO_3$-saturated water	1, 3, 10, 30, 100, 300, 1000, 3000	-
i173	0/100	5	$CaCO_3$-saturated water	1, 3, 10, 30, 100, 300, 1000, 3000	-
i058	100/0	5	$CaCO_3$-saturated water	-	0.1, 0.3, 1, 3, 10, 30, 100, 300, 1000
i184	95/5	5	$CaCO_3$-saturated water	-	0.1, 0.3, 1, 3, 10, 30, 100, 300, 1000
i185	80/20	5	$CaCO_3$-saturated water	-	0.1, 0.3, 1, 3, 10, 30, 100, 300, 1000
i186	50/50	5	$CaCO_3$-saturated water	-	0.1, 0.3, 1, 3, 10, 30, 100, 300, 1000
i183	100/0	5	$CaCO_3$-saturated water	-	0.1, 0.3, 1, 3, 10, 30, 100, 300, 1000
i234	95/5	50	$CaCO_3$-saturated water	1, 3, 10, 30, 100, 300, 1000, 3000	1, 3, 10, 30, 100, 300, 1000
i235	95/5	20	$CaCO_3$-saturated water	1, 3, 10, 30, 100, 300, 1000, 3000	1, 3, 10, 30, 100, 300, 1000
i236	80/20	50	$CaCO_3$-saturated water	1, 3, 10, 30, 100, 300, 1000, 3000	1, 3, 10, 30, 100, 300, 1000
i237	80/20	20	$CaCO_3$-saturated water	1, 3, 10, 30, 100, 300, 1000, 3000	1, 3, 10, 30, 100, 300, 1000
i161	100/0	5	Silicone Oil	1, 3, 10, 30, 100, 300, 1000, 3000	-
i262	95/5	5	Silicone Oil	1, 3, 10, 30, 100, 300, 1000, 3000, 1000, 300, 100	-

[a]All experiments were conducted at a background sliding velocity of 10 μm/s.

friction measured upon reshear after each hold and the prehold steady state friction ($\Delta\mu$), as in previous work by *Marone* [1998], *Richardson and Marone* [1999], and *Frye and Marone* [2002]. Steady state friction is generally identical before and after the hold. However, few samples showed a slight strain-related trend in plotting friction as a function of shear strain. We removed these trends in order to measure a more precise $\Delta\mu$. Frictional healing rates (β) was calculated as

$$\beta = \Delta\mu/\Delta\log_{10}(t_h) \tag{1}$$

During velocity-stepping tests, we imposed velocity step sequences of 0.1 to 1000 μm/s with a constant displacement of 750 μm at each step. In four experiments we also ran velocity step sequence of 1 to 1000 μm/s after the slide-hold-slide sequence. Each velocity step consists of a near-instantaneous step changes in sliding velocity from V_0 to V [e.g., *Dieterich*, 1979; *Marone*, 1998; *Scholz*, 1998]. For each velocity step, the velocity was stepped up and the new sliding velocity held constant until a new steady state shear stress level was attained (Figures 1c and 1e). The instantaneous change in friction scales as the friction parameter $a\ln(V/V_0)$, where a is an empirical constant defined as the direct effect [e.g., *Ruina*, 1983]. The subsequent drop to a new steady state value of friction scales as the friction parameter $b\ln(V/V_0)$, where b is an empirical constant defined as the evolution effect [e.g., *Ruina*, 1983]. The velocity dependence of steady state friction ($a-b$) is defined as

$$a-b = \frac{\Delta\mu_{ss}}{\ln(V/V_0)} \tag{2}$$

where $\Delta\mu_{ss}$ is the change in steady state friction. Positive values of ($a-b$), defining velocity-strengthening behavior, indicate that stable sliding should be expected. Negative values of ($a-b$), i.e., velocity-weakening behavior, are a requirement for the nucleation of slip instability [e.g., *Dieterich and Kilgore*, 1994; *Marone*, 1998; *Scholz*, 1998].

The collected data were subsequently modeled with the Dieterich time-dependent version of the rate and state friction constitutive law and evolution equation [*Dieterich*, 1979]

$$\mu = \mu_0 + a\ln\left(\frac{V}{V_0}\right) + b\ln\left(\frac{V_0\theta}{D_C}\right), \frac{d\theta}{dt} = 1 - \frac{\theta V}{D_C} \tag{3}$$

where V_0 is a reference velocity and μ_0 is the steady state friction at $V = V_0$. D_c is the critical slip distance and θ is the state variable (units of time) that expresses the effective contact time derived from the ratio of a critical

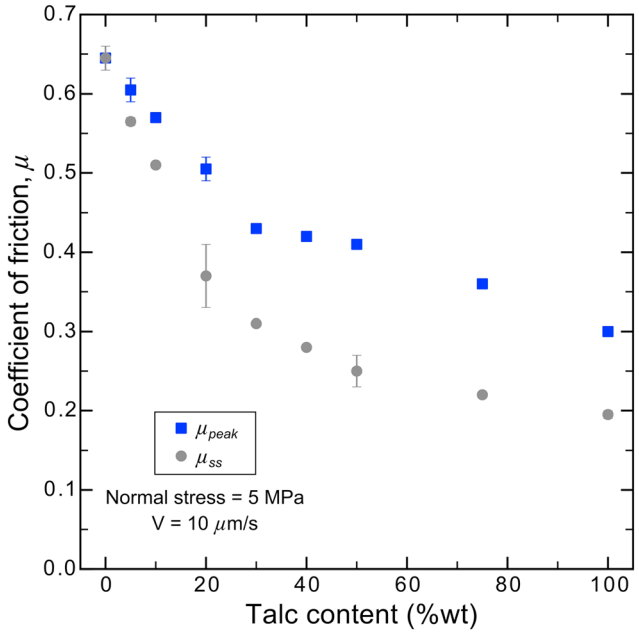

Figure 2. Friction of talc/calcite binary mixtures as function of talc content in experiments carried out at sliding velocity of 10 μm/s and at constant normal stress of 5 MPa. Friction systematically decreases with increasing talc content. The values reported for 0%, 5%, 20%, 50%, and 100% are the average between slide-hold-slide experiments and velocity step experiments, the error bar thus indicates the difference between the two values, whereas the values reported for all the other mixtures result from slide-hold-slide experiments. For the strain and the displacement at which the values were measured see Figure S3.

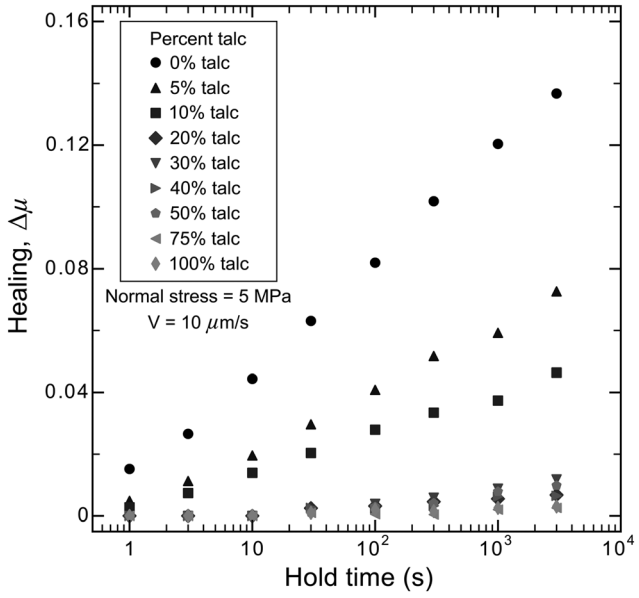

Figure 3. Frictional healing as function of hold time for different talc contents in experiments carried out at sliding velocity of 10 μm/s and at constant normal stress of 5 MPa. A small amount of talc strongly reduces frictional healing.

slip distance D_c to slip velocity V. The state variable θ is thought to represent the average lifetime of asperity contacts that control friction, and the critical slip distance D_c represents the displacement over which the population of asperity contacts are renewed [*Marone and Kilgore*, 1993; *Scholz*, 1998]. To model our data, the constitutive law and the evolution equation are coupled with an equation describing the compliant coupling between the frictional surface and its surroundings, i.e., the interaction of the sample with its elastic load frame

$$\frac{d\mu}{dt} = k\left(V_{lp}/V\right) \quad (4)$$

where V_{lp} is the velocity measured at the displacement control point and k is stiffness of the testing apparatus and the sample blocks, normalized by the normal stress, in units of coefficient of friction per displacement. We simultaneously solved the Dieterich constitutive law and evolution equation, with elastic coupling equation as a constraint, by using a fifth-order Runge-Kutta numerical integration. The constitutive parameters a, b, and D_c were obtained as best fit parameter values using an iterative, least squares method to solve the nonlinear inverse problem [e.g., *Reinen and Weeks*, 1993; *Blanpied et al.*, 1998; *Saffer and Marone*, 2003].

At the end of the slide-hold-slide tests, parts of the gouge layers were collected, dried at room temperature, and preserved in epoxy resin, in order to obtain thin sections parallel to the sense of shear for microstructural analysis.

2.3. Microscopy Observations

Microstructural observations were performed with a JEOL JSM-6500 F thermal field emission scanning electron microscope, installed in the Electron Microscopy Laboratory at the INGV in Rome, Italy. All the micrographs presented in this manuscript are backscattered electron images. Specifically, we collected photo mosaics at high magnification of the entire thin section thickness and micrographs of thin section details at higher magnification.

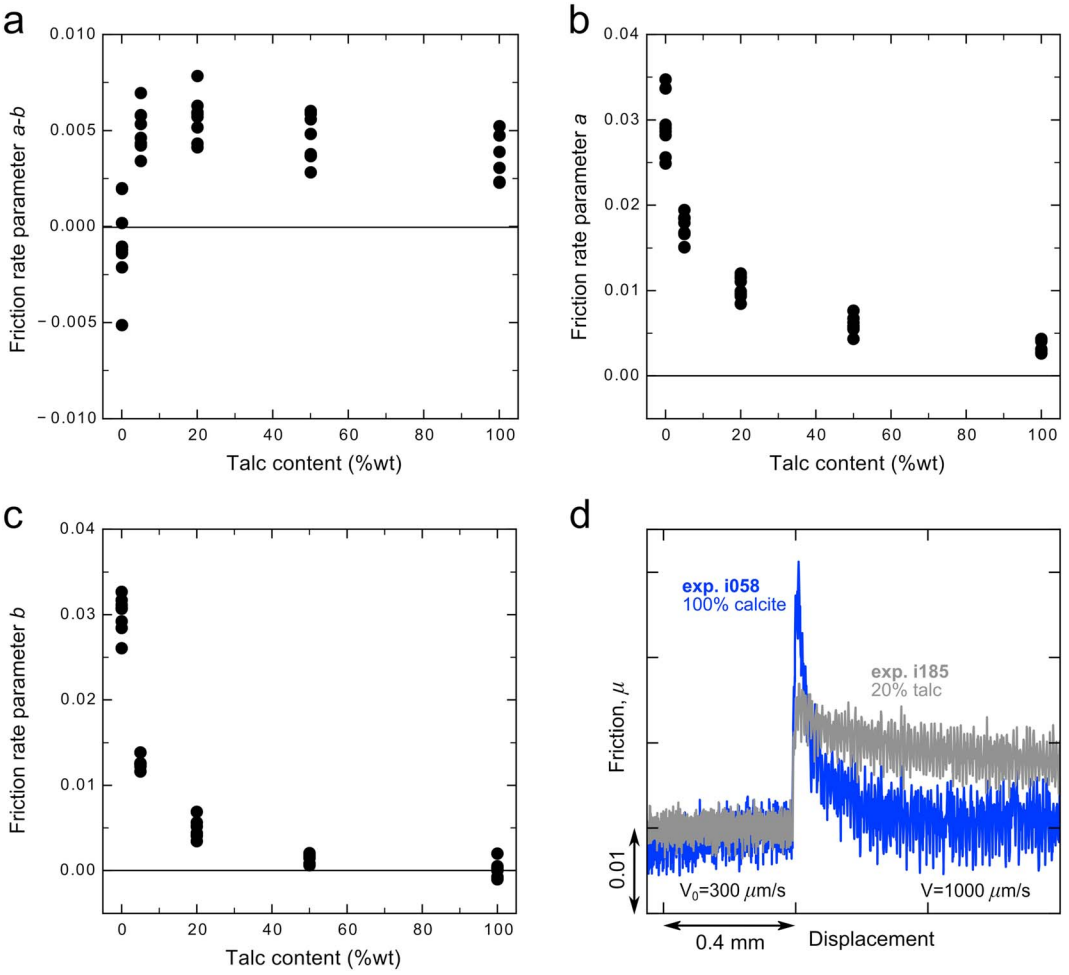

Figure 4. Friction rate parameters as function of talc content in experiments carried out at 5 MPa of normal stress. (a) Talc/calcite mixtures are characterized by velocity-strengthening frictional behavior, i.e., positive ($a - b$). (b) The "direct effect" a decreases with increasing talc content. (c) The "evolution effect" b decreases with increasing talc content approaching negative values. (d) A comparison between the velocity dependence of 100% calcite gouge (blue) and 20% talc gouge (gray) at 5 MPa for a velocity step of 300–1000 μm/s.

3. Results

3.1. Mechanical Data

3.1.1. Frictional Behavior at 5 MPa Normal Stress

Our strength results, with the exception of pure calcite, indicate an evolution curve of the coefficient of friction characterized by a distinct peak (μ_{peak}) and subsequent decay to a steady state value (μ_{ss}) with increasing displacement (Figures 1a and S3b). All the values of steady state friction reported and discussed hereafter are measured during slide-hold-slide experiments. All the mixtures, at a sliding velocity of 10 μm/s, have values of the coefficient of friction that range between pure calcite value, i.e., $\mu_{peak} = \mu_{ss} \approx 0.66$ and pure talc value, i.e., $\mu_{peak} \approx 0.30$ and $\mu_{ss} \approx 0.20$ (Figure 2). The coefficient of friction decreases systematically with increasing talc content, but the trend of friction reduction between the two end-members is not linear. There is a significant drop in friction (70% in μ_{ss}) between 0 and 20% talc, and a more gradual decrease at higher talc concentrations. In addition, the difference between peak friction and steady state friction tends to increase from 0 to 0.18 with the progressive addition of up to 50% talc and then to decrease slightly for higher talc contents. Strain at which the coefficient of friction reaches peak values tends to increase with increasing talc content, from $\gamma = 0.85$ to $\gamma = 1.88$, whereas strain at which friction reaches steady state values tends to slightly decrease with increasing talc content, from $\gamma = 6.41$ to $\gamma = 1.88$ (Figure S3a).

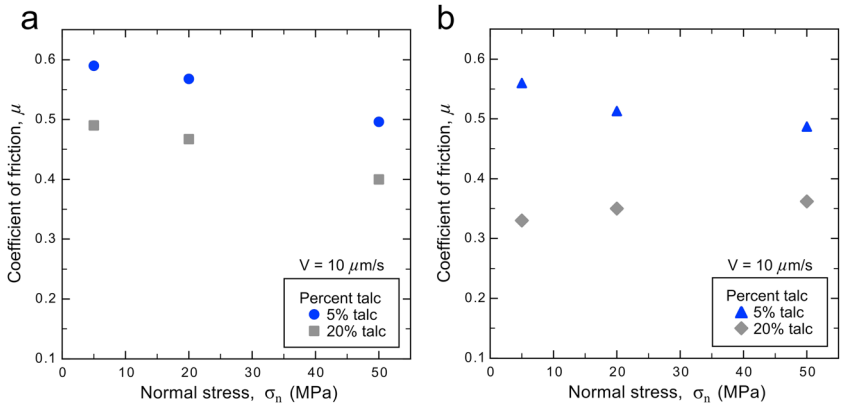

Figure 5. (a) Peak friction and (b) steady state friction of talc/calcite binary mixtures as a function of normal stress at talc contents of 5 and 20%. Experiments were carried out at a sliding velocity of 10 μm/s.

Figure 3 shows healing results for our experiments at normal stress of 5 MPa. A content of 5% of talc is enough to cause a 50% drop in the rate of frictional healing, i.e., from $\beta \approx 0.0361$ to $\beta \approx 0.0196$. The healing rate of 10% talc sample is lower ($\beta \approx 0.0124$) and it is nearly zero for samples containing ≥20% talc. In samples with talc ranging from 20% to 50%, the rate of frictional healing ranges from $0.0021 < \beta < 0.0035$. For the gouges containing 75% and 100% talc the healing rate is $\beta \approx 0.0010$. Like for frictional strength, there is a significant and sharp, almost linear, drop in healing rate between 0 and 20% talc, and a slower degradation at higher talc contents.

Concerning the velocity dependence of friction (Figure 4), pure calcite gouge shows variable behavior from velocity strengthening to velocity weakening, whereas all the other gouges exhibit a clear velocity-strengthening behavior (Figure 4a). The trend of $(a - b)$ with increasing talc content grows up to 20% talc, with maximum value $(a - b) \approx 0.0079$ (velocity step 100–300 μm/s). Subsequently, $(a - b)$ slowly decreases up to 50% talc ($0.0016 < (a - b) < 0.0061$), and then remains almost constant. The friction rate parameter *a*, as well as the friction rate parameter *b*, decreases with increasing talc content (Figures 4b and 4c). The major drop in *a* and *b* is recorded between 0 and 20% of talc. The *b* value then remains close to zero with some negative values for the velocity steps 30–100 μm/s, 100–300 μm/s, and 300–1000 μm/s in the pure talc sample. In Figure 4d we show a velocity step, 300–1000 μm/s, conducted on the pure calcite and on the 20% talc gouges: here we can observe the decrease in *a* values and the reduction of the *b* values to zero in response to an addition of 20% talc to pure calcite.

3.1.2. Frictional Behavior at 20 and 50 MPa Normal Stress

Mechanical results from the first suite of 14 experiments at 5 MPa highlight the presence of a threshold value corresponding to a talc content of 20%. In the calcite/talc series, most of the degradation in friction, healing rate, and *a* and *b* parameters occurs by 20% talc. Moreover, our slide-hold-slide experiments showed that a content of 5% talc is enough to halve the healing rate of calcite gouge. In order to better constrain the frictional properties of 5 and 20% talc gouges, we performed four additional experiments at higher normal stresses (i.e., 20 or 50 MPa).

The coefficient of friction of the 5% talc sample is systematically reduced with increasing normal stress (Figure 5): the 5% talc sample at 5 MPa has $\mu_{peak} \approx 0.59$ and $\mu_{ss} \approx 0.55$, whereas at 50 MPa has $\mu_{peak} \approx 0.50$ and $\mu_{ss} \approx 0.49$. The coefficient of friction of the 20% talc gouge shows a strong reduction in the difference between peak friction and steady state friction with increasing normal stress. The peak friction of the 20% talc sample systematically decreases from $\mu_{peak} \approx 0.49$ at 5 MPa to $\mu_{peak} \approx 0.40$ at 50 MPa (Figure 5a), whereas the steady state friction increases from $\mu_{ss} \approx 0.33$ at 5 MPa to $\mu_{ss} \approx 0.36$ (Figure 5b).

In Figure 6a we show healing values of 5 and 20% talc samples at different normal stresses versus hold time. Gouges with 5% talc show remarkably different healing values, $\Delta\mu$, at higher normal stresses: the rate of frictional healing decreases with increasing normal stress ranging from $\beta \approx 0.0196$ at 5 MPa to $\beta \approx 0.0032$ at 50 MPa. In Figure 6b, we report the different healing behavior of a 5% talc gouge at different normal stresses during a 3000 s hold: at 5 MPa, $\Delta\mu \approx 0.07267$, whereas at 20 MPa, $\Delta\mu \approx 0.01473$. The higher normal stress seems to suppress healing. Conversely, in a gouge with 20% talc, healing has no normal

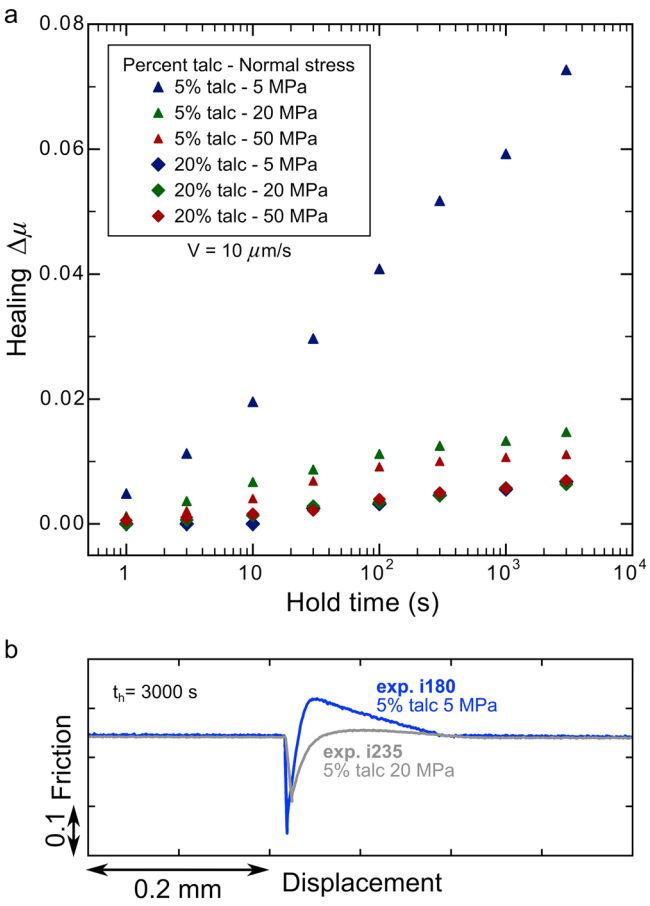

Figure 6. (a) Frictional healing as function of hold time, talc content (5% and 20% talc) and normal stresses (5 MPa, 20 MPa, and 50 MPa) in experiments carried out at a sliding velocity of 10 μm/s. Frictional healing of the 5% talc sample is strongly affected by changes in normal stress. (b) Comparison between the healing of 5% talc gouge at 5 MPa normal stress (blue) and at 20 MPa normal stress (gray) in a 3000 s hold.

stress dependence: healing rate is almost constant with $\beta \approx 0.0021$ at 5 MPa and $\beta \approx 0.0018$ at both 20 and 50 MPa.

At 20 and 50 MPa, we observe velocity-strengthening behavior with $(a-b)$ values similar to values obtained at 5 MPa (Figure 7a). Gouge with 5% talc at 50 MPa has the most variable $(a-b)$ values, ranging from 0.0042 to 0.0107. Moreover, at 50 MPa normal stresses, $(a-b)$ systematically decreases with increasing velocity, whereas friction rate parameters a and b systematic increase with increasing velocity. In the 5% talc sample, the friction rate parameter a (Figure 7b) slightly decreases with increasing normal stress, ranging from $0.0151 < a < 0.0194$ to $0.0082 < a < 0.0133$. In the 20% talc sample, the reduction in a with increasing normal stress is less evident. The parameter b (Figure 7c) shows a decrease between 5 and 20 MPa for both 5 and 20% talc gouges, whereas the b values at 50 MPa are more variable, becoming negative in some velocity steps ($b \approx -0.0025$ for 5% talc in velocity step 1–3 μm/s, $b \approx -0.0019$ for 20% talc in velocity step 1–3 μm/s). In Figure 7d we show two velocity steps conducted on the 5% talc gouge at different normal stresses: at 5 MPa velocity-dependent behavior is characterized by positive a and positive b in both velocity steps 1–3 μm/s and 100–300 μm/s, whereas at 50 MPa velocity-dependent behavior shows different b parameter values, changing from negative b in velocity step 1–3 μm/s to positive b in velocity step 100–300 μm/s.

3.2. Microstructural Observations

Scanning electron microscopy investigations on the experimental faults at low normal stress, i.e., 5 MPa, indicate that deformation-induced microstructures are strongly controlled by the amount of talc. The texture of pure calcite sample (Figure 8a) is dominated by angular grains, isotropically distributed in a finer matrix. Overall, the structure is characterized by limited portions of fine-grained calcite, possibly derived from both localized cataclasis and/or starting material. We observe limited fracturing and chipping [e.g., *Billi*, 2010] of larger calcite grains. The starting calcite grain size distribution shows a high concentration of fine material (50% of the volume is characterized by a grain size < 16 μm; Figure S1), which is clearly displayed in thin sections taken from samples after only the application of normal stress (Figure S2). We suggest that in our saturated samples and at low normal stress, the deformation occurs via cataclastic flow, with grain rotation, translation, and frictional sliding at grain contacts, with the development of few areas of fine-grained calcite. These discontinuous zones can develop from the portions of the starting material characterized by small grain sizes and do not testify a predominant role of grain size reduction during deformation.

In the 5% talc sample (Figures 8b and 8d), the texture is still homogeneous and dominated by a minor amount of large calcite grains (grain size > 100 μm). Calcite grains are more rounded in comparison to the

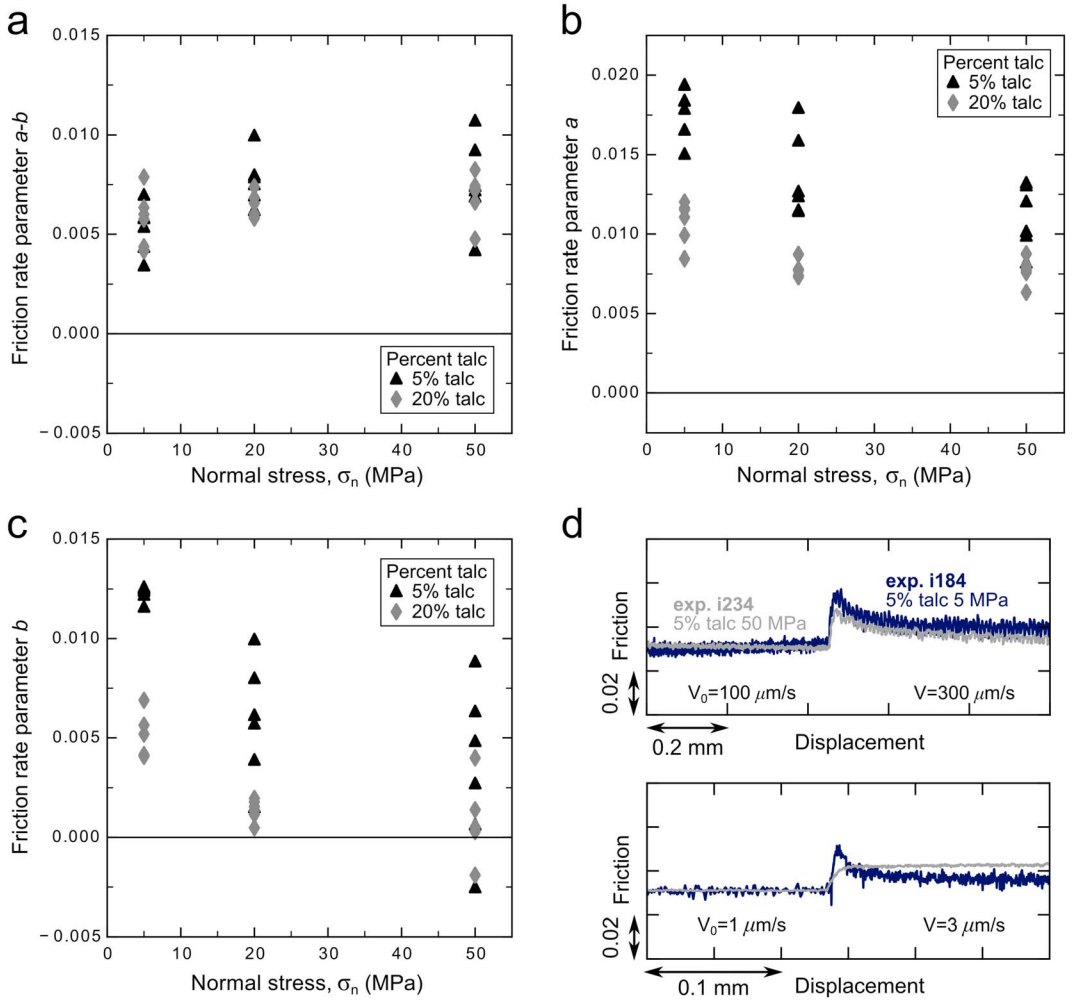

Figure 7. Friction rate parameters as function of normal stress (5 MPa, 20 MPa, and 50 MPa) and talc content (5% and 20%). (a) Talc/calcite mixtures are characterized by velocity-strengthening frictional behavior, i.e., positive ($a - b$). (b) The "direct effect" a decreases with increasing normal stress. (c) The "evolution effect" b decreases with increasing normal stress approaching negative values. (d) Comparison between the velocity dependence of 5% talc gouge at 5 MPa normal stress (blue) and at 50 MPa normal stress (gray) for velocity steps of 100–300 μm/s and 1–3 μm/s.

pure calcite gouge, suggesting a grain size reduction process such as chipping [*Billi*, 2010]. Talc lamellae are scattered in the bulk microstructure, partially coating calcite grains and iso-orienting themselves, forming a sort of "protofoliation" (Figure 8d).

The microstructure of the 20% talc sample (Figures 8c and 8e) suggests a mixed mode of deformation with distributed deformation along the bulk microstructure and localization occurring along shear planes, defined on the basis of their geometric relationship to the YPR fabric described by *Logan et al.* [1992]. Talc flakes scattered in the bulk microstructure are organized into foliation and are occasionally deformed by kinking and folding. R_1 shear planes show an enrichment of talc flakes and fine-grained calcite. The development of an interconnected network of talc lamellae around fine-grained calcite enables focusing of strain along shear planes. R_1 shear planes (Figure 8e), ~10° clockwise oriented to the shear plane, are characterized by a high concentration of talc lamellae and the surrounding calcite grains display internal brittle deformation enhanced by the high strain condition. The continuity of R_1 planes is high, whereas Y planes, parallel to the shear plane, tend to be more discontinuous. Talc lamellae alignments can also be observed also along P foliation planes, ~145° clockwise to the shear plane.

Our microstructural analysis shows that increasing talc content results in a progressive microstructural organization. The mechanism of deformation evolves from distributed cataclastic flow (0–5% of talc) to

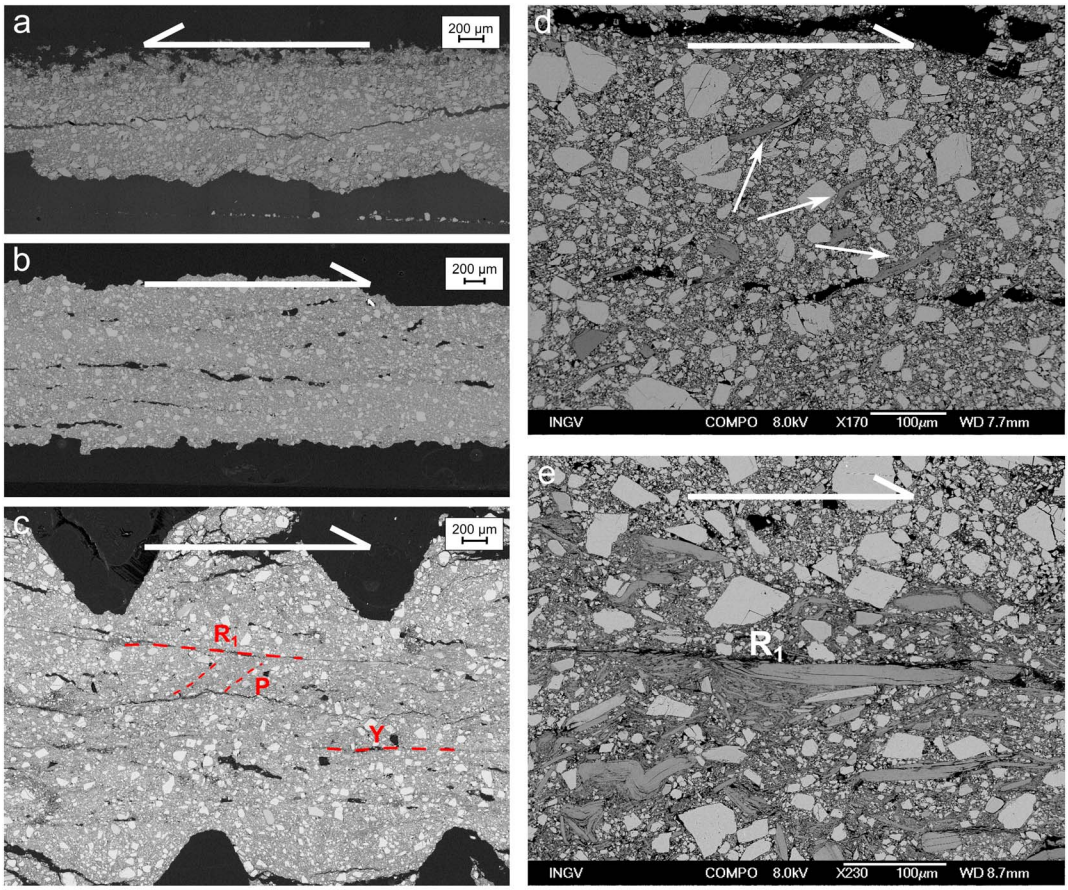

Figure 8. SEM micrograph showing microstructures developed in samples with variable talc content. (a) Distributed deformation characterizes the pure calcite sample, $\gamma \approx 7.1$. (b) The 5% talc sample deformed predominantly by cataclastic flow, $\gamma \approx 10.5$. (c) The 20% talc sample localizes deformation along shear zones, with the YPR fabric described by *Logan et al.* [1992]. The shear strain is $\gamma \approx 7.4$. (d) Detail of the 5% talc sample showing talc lamellae iso-orientation (white arrows). (e) Detail of the 20% talc sample showing R_1 shear zone localized on talc lamellae.

localized frictional sliding along talc-rich R_1 shear planes (20% of talc) with some grain size reduction and redistribution of finer calcite grains along shear planes, to distributed frictional sliding along talc-rich domains (50% of talc).

4. Discussion

4.1. Integration of Mechanical Data and Microstructures

Peak and steady state frictional strengths decrease at two different rates (Figure 2). For both, a talc content of 20% is the value that marks a significant change in the degradation rate: a more rapid decrease at talc contents between 0%–20% is followed by a slower decrease from 20% to 100%. A talc content of 20% also strongly influences frictional healing (Figure 3) and velocity dependence (Figure 4). One possible explanation for this weakening trend is the generation of overpressure resulting from the decreasing permeability of gouges with increasing talc content. However, this mechanism unlikely provides a strong contribution to the weakening of our talc-bearing gouges, for mainly two reasons: our experiments were conducted under drained conditions, which allow the dissipation of any generated overpressure at least over the experiment time span, and the addition of only 5% of talc, which results in a decrease in friction, unlikely affects permeability parallel to the gouge such that overpressure would develop. Ruling out fluid overpressure as a weakening mechanism, on the grounds of microstructural observations we indicate the occurrence of shear localization on talc-enriched planes as the mechanism able to explain the variation in the frictional properties with increasing talc content.

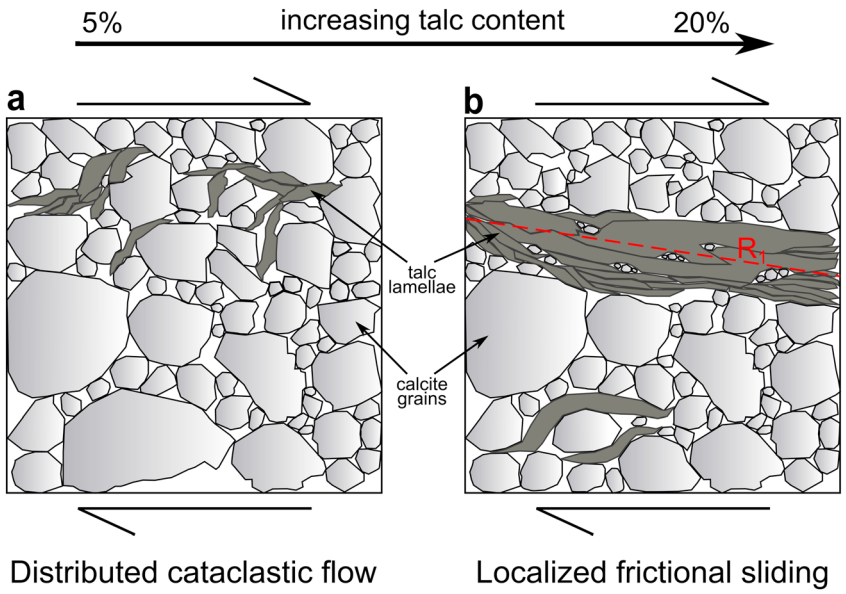

Figure 9. (a) A stress-supporting framework of calcite grains, with talc lamellae (5% wt) situated between some calcite grains, characterized by distributed deformation and resulting in high frictional strength, high frictional healing, and high rate parameters. (b) As the talc fraction increases, the development of interconnected talc network localizes deformation on planes (e.g., R_1) and reduces the frictional strength, the frictional healing, and the rate parameters.

At low talc concentrations (0–10%), the absence of continuous gouge portions characterized by a concentration of small calcite grains suggests no localization of grain size reduction nor grain size redistribution along shear bands. The overall lower amount of 100 μm sized calcite grains and their more rounded shape in the 5 and 10% talc samples, when compared to the pure calcite gouge, can be interpreted as an enhanced grain size reduction due to the incipient development of talc foliation. The progressive alignment of talc lamellae is favored in regions where calcite grain size is reduced, progressively localizing the strain. However, in our low talc concentration gouges, this mechanism seems to not have a predominant role as demonstrated by a limited number of intragrain fractures within calcite grains. In addition, short and discontinuous alignments of talc (Figures 8b and 8d) indicate that the amount of talc is not enough to localize the shear. On the basis of all these observations, we can infer that distributed cataclastic flow is the main deformation mechanism (Figure 9a). These gouges are relatively strong, with μ_{ss} ranging between 0.66 and 0.51 at 5 MPa, and the frictional healing is relatively high, with a healing rate β ranging between 0.036 and 0.012. The friction rate parameter a is high, with values ranging between 0.035 and 0.015. The direct effect a results from a change in gouge strength upon a velocity step, first attributed to a rate dependence of contact strength [e.g., *Dieterich*, 1979]. However, any porosity change in response to a velocity step influences gouge strength and consequently the a value. Moreover, different mechanisms, such as pressure solution and plasticity at grain contacts, can indirectly contribute to a values, influencing the properties of grain contacts and the porosity of our gouges. Dilatancy effects in gouge layers due to a step change in sliding velocity have long been recognized [e.g., *Marone et al*., 1990; *Sammis and Steacy*, 1994; *Mair and Marone*, 1999]. Dilation of gouges rich in calcite, resulting from the rearrangement of the microstructure in response to a step to higher sliding velocity, consists in grains sliding and rotation and involves an increase in friction due to work expended against the normal stress. In our mixtures, calcite dilation influences the mixture behavior during slide-hold-slide experiments (Figure S4): the dilation of the 5% and the 20% talc samples are reduced, respectively, by about 40% and 60%, when compared with the pure calcite sample. The high dilation values associated with high healing values upon reshear suggests a possible contribution of dilation, related to granular calcite, in the evolution of the a values with increasing talc. Nonetheless, time-dependent mechanisms, such as pressure solution and plasticity at contacts can contribute to the direct effect. Pressure solution, strengthening at grain contacts, correlates positively with a values. Conversely, plasticity limits dilation resulting in lower a values. However, as shown by other experiments that we performed on calcite gouges (B. M. Carpenter, et al., The influence of normal stress and sliding velocity on the frictional behavior of calcite at room temperature: Insights from laboratory experiments and microstructural observations,

submitted to *Geophysical Journal International*, 2015), plasticity in calcite gouges, at room temperature, is an effective mechanism only at low slip velocities and high normal stresses, excluding an important contribution of plasticity in our low stress data set. Furthermore, the large friction rate parameter b in calcite-rich gouges can be explained by the attainment of a new steady state porosity following the microstructure rearrangement through granular dilation.

The 20% talc sample shows a YPR geometry [*Logan et al*., 1992] of the experimental gouge layer (e.g., Figure 8c) with talc lamellae concentrated along R_1 shear planes. This microstructure favors a deformation mechanism characterized by frictional sliding along the talc foliae (Figure 9b), typically observed in pure talc shear experiments [e.g., *Boutareaud et al*., 2012; *Misra et al*., 2014], promoting a decrease in the frictional strength to values of μ_{ss} ranging between 0.33 and 0.20. Similarly, *Moore and Lockner* [2011] in quartz/talc mixtures observed a marked weakening resulting from the formation of R_1 planes that cross the entire sample. Moreover, *Hirauchi et al*. [2013], shearing a mixture of antigorite and quartz at different experimental conditions generating different amounts of metasomatically grown talc, observed a weakening of the gouge associated with the progressive development of talc along through-going boundary shears. The almost zero healing of the gouges, with β smaller than 0.002, suggests that during hold periods the growing contact area, if it occurs, does not result in an increase in frictional strength. Talc lamellae, with their platy shape, can hinder growth of contact area. Following this interpretation, our data are in agreement with previous studies on phyllosilicates-rich fault rocks that have suggested real contact areas saturation in the actively slipping zone, due to crystal habit, as mechanism for inhibiting frictional healing [e.g., *Bos and Spiers*, 2001; *Saffer and Marone*, 2003; *Tesei et al*., 2012]. The localization of deformation along interconnected, talc-rich shear surfaces coincides with the onset of a strong velocity-strengthening behavior, as previously observed in phyllosilicate-bearing gouges that developed a strong foliation [e.g., *Bos and Spiers*, 2002; *Niemeijer and Spiers*, 2005; *Niemeijer and Spiers*, 2006]. In these previous works, the strong foliation allowed the attainment of a steady state microstructure that does not require dilation upon a step to higher shearing velocity. Similarly, the development of connected, talc-rich shear surfaces where deformation is highly localized does not require any significant rearrangement upon a sudden change in velocity, favoring velocity-strengthening behavior. Specifically, the friction rate parameters a and b decrease with increasing talc content (Figures 4b and 4c): again a 20% talc content marks the larger change in the evolution of the rate parameters. We suggest that, by adding more and more talc along the experimental fault, cataclastic flow of granular calcite is overcome by frictional sliding along the platy talc, resulting in a less pronounced dilatancy effect, thus reducing a values. In addition, previous studies [*Beeler et al*., 2007] proposed dislocation glide at room temperature as a possible mechanism operating in talc and other phyllosilicates. Such a mechanism possibly controls the value of the direct effect in our samples containing $\geq$20% of talc. Furthermore, in talc-rich samples, the talc lamellae are almost in complete contact, causing a decrease of b to near zero, implying that the real area of frictional contact does not change after a velocity step [e.g., *Scholz*, 2002; *Niemeijer et al*., 2010; *Collettini et al*., 2011].

With increasing normal stress our experiments at 5 and 20% talc contents show a more pronounced shift toward a pure talc-like behavior, that is, (a) a reduction in the difference between peak and steady state friction in particular for 20% of talc (Figure 5); (b) a close to zero healing rate for 5% of talc (Figure 6); and (c) a reduction in the direct effect and an even stronger reduction in the evolution effect resulting in a stronger velocity-strengthening behavior (Figure 7). With increasing normal stress, the decrease in steady state friction in the 5% talc versus the increase in steady state friction in the 20% talc can result from the different contributions of grain size reduction to the deformation mechanisms operating in these gouges. Gouges with 5% talc, in which the deformation is predominantly accommodated by distributed cataclastic flow at low normal stress, can be weakened at higher normal stresses by the occurrence of grain size reduction that enhances the localization of deformation along shear bands. On the other hand, gouges with 20% talc that deform by localized frictional sliding along talc-rich surfaces, can be strengthened by the involvement of small size grain, deriving from comminution, in the shear zones, as already proposed in previous studies on clay-rich gouges [*den Hartog et al*., 2012]. However, since the increase in steady state friction in the 20% talc is rather slight and the values can be considered almost constant, another likely explanation for the two different trends in Figure 5b can be related to the effect of cohesion. Fitting the shear stress versus normal stress data with the Coulomb-Mohr failure criterion, we obtained a cohesion of $C \approx 0.5$ MPa for the 5% talc sample and an almost zero cohesion for the 20% talc sample. Since we calculated

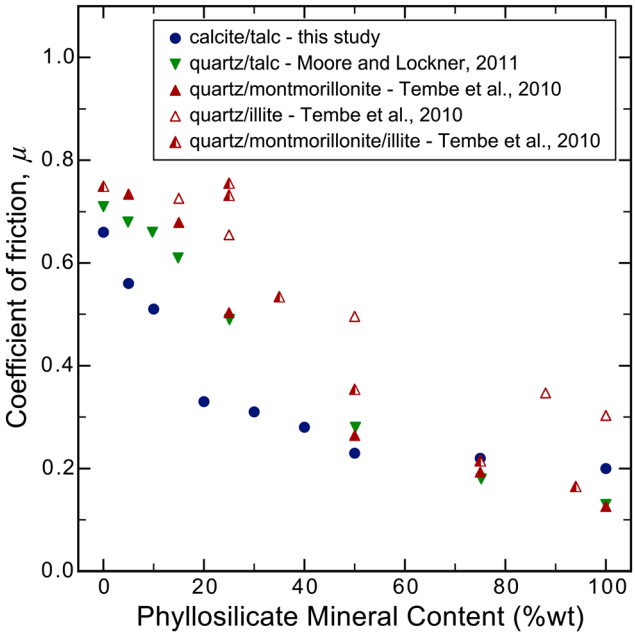

Figure 10. Comparison of friction degradation trends from different gouge mixtures. *Moore and Lockner* [2011] conducted experiments at high temperature (200°C); however, quartz solubility at high temperature is comparable to calcite solubility at room temperature [*Rimstidt*, 1997]. Fault-parallel displacements are also comparable: *Moore and Lockner* [2011] measured the coefficient of friction at 4 mm, *Tembe et al.* [2010] at about 9 mm, whereas in our experiments the steady state is reached between 5 and 8 mm. Quartz/talc [*Moore and Lockner*, 2011] and quartz/montmorillonite [*Tembe et al.*, 2010] mixtures show similar trends that differ from our calcite/talc mixtures for low phyllosilicates contents. Quartz/illite mixture [*Tembe et al.*, 2010] shows an almost linear trend.

the steady state friction as the ratio between τ and σ_n, an amount of cohesion of ~0.5 for the 5% talc sample results in an apparent decrease of the friction value of ~0.09 between $\sigma_n = 5$ MPa and $\sigma_n = 50$ MPa, consistent with the measured steady state values (Figure 5b). The 20% talc sample, having $C \approx 0$ MPa, does not show any contribution of cohesion to the friction values.

To summarize, our results documented the significant drop in frictional strength, healing rate, and rate parameters between 0% and 20% of talc due to the progressive localization of deformation on discrete talc-rich surfaces.

4.2. Comparison to Previous Data

The frictional strength for pure calcite is consistent with results from other studies on limestone and calcite-rich fault rock at low stress and room temperature [e.g., *Weeks and Tullis*, 1985; *Scuderi et al.*, 2013; *Carpenter et al.*, 2014; *Tesei et al.*, 2014; *Verberne et al.*, 2014]. For pure talc, our data are in good agreement with results from other experiments conducted on synthetic talc gouges at variable normal stress and temperature representative of the shallow crustal conditions [e.g., *Escartín et al.*, 2008; *Moore and Lockner*, 2008; *Niemeijer et al.*, 2010; *Hirauchi et al.*, 2013]. Binary mixtures of calcite and talc show stress-strain curves characterized by a maximum value of strength reached during the "run-in" phase followed by a decrease in friction, up to 0.2, with increasing strain (Figures 1 and 2). This evolution is typical of clay-dominated gouges and is generally explained by the alignment of clay particles with increasing deformation [e.g., *Lupini et al.*, 1981; *Chester and Logan*, 1987; *Bos and Spiers*, 2001; *Saffer et al.*, 2001; *Saffer and Marone*, 2003; *Moore and Lockner*, 2004; *Tembe et al.*, 2010].

In the following we present a comparison between our friction data on binary mixtures of talc and calcite with other frictional strength data of mixtures of quartz and various phyllosilicates [*Tembe et al.*, 2010; *Moore and Lockner*, 2011]. In this way we try to characterize the interplay between strong and angular material, such as quartz and calcite, and weak and platy minerals, such as talc and clays, in frictional strength. Comparing our 5 MPa data set with studies conducted at higher normal stress is reasonable considering that (1) the effect of normal stress on the coefficient of friction in our experiments is small, i.e., the variation of steady state friction is less than 0.1 for different talc contents and normal stresses (Figure 5b); (2) we are presenting a conservative estimate of minimum talc amount able to weaken a fault, because for small talc percentages (5–20%) the increase of normal stress changes the rate and state parameters toward a more talc-like behavior (Figures 5–7).

Tembe et al. [2010] interpreted their strength data in terms of three regimes [*Lupini et al.*, 1981]. Close to the end-members composition, the coefficient of friction is essentially the same of the respective end-member, whereas it decreases with increasing clay content at intermediate compositions. *Moore and Lockner* [2011] presented frictional data on quartz and talc mixtures showing that gouges containing low talc percentage fall on a straight line connecting the end-member values, whereas the rest of the mixtures follows a curved trend below the line. Our data mainly differ from these studies in the degradation trend at low talc content. In

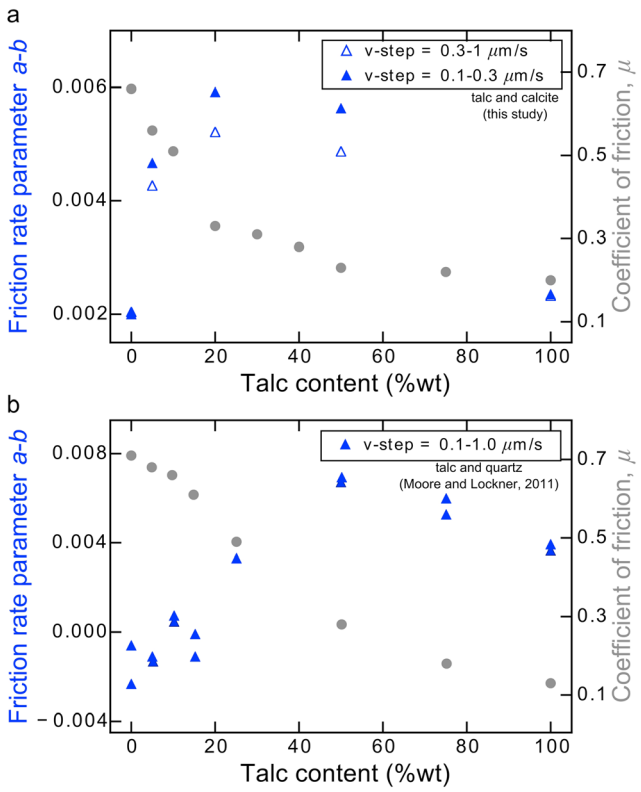

Figure 11. Comparison between friction reduction trend and $(a - b)$ trend with increasing talc content. (a) In our data, an initial fast drop in friction corresponds to an increase in $(a - b)$ parameter. (b) Data from *Moore and Lockner* [2011] also show that a rapid decrease in friction corresponds to an increase in $(a - b)$ parameter. We selected the 0.1–0.3 μm/s and the 0.3–1.0 μm/s velocity steps from our data set in order to compare our results to *Moore and Lockner's* [2011] 0.1–1.0 μm/s velocity steps.

particular, we observe an initial linear rapid decrease in friction, between 0 and 20% talc, followed by a more gradual decrease at talc contents above 20%. Specifically, in these previous data sets, the onset of a fast degradation rate occurs with the addition of a certain amount of phyllosilicates to quartz gouges (i.e., 15% in the case of illite, montmorillonite, and talc, and 25% in the case of montmorillonite/illite). Before these thresholds the degradation rate is slower. Our data set is slightly different since the onset of the fast degradation rate coincides with the addition of low amounts of talc, i.e., 5%. Consequently, we do not observe a slower rate before the onset of the fast decrease in friction. The grain size of starting materials can be a possible explanation for the different trends documented (Figure 10). *Tembe et al.* [2010] and *Moore and Lockner* [2011] used nonoverlapping grain sizes of end-member minerals: respectively, <175 μm sized quartz and <3 μm sized montmorillonite, <180 μm sized quartz and <90 μm sized talc. The different frictional behavior of binary mixtures can be justified by an ideal packing model, as in previous works [*Lupini et al.*, 1981; *Tembe et al.*, 2010]. In mixtures characterized by nonoverlapping grain sizes, at low clay concentrations, the smaller-sized clay lamellae are isolated and concentrated only in the void spaces. In this situation the stress-supporting framework of quartz grains determines high strength values. Instead, in our experiments all the starting materials were sieved to a size <125 μm and have a similar volumetric grain size distribution (Figure S1). In this case, even at very low phyllosilicate content, talc lamellae cannot be isolated in void spaces but they separate calcite grains interfering with the calcite grain-grain framework (Figure 9a) and thus reducing friction. As a result, the first, high frictional strength regime of *Lupini et al.* [1981] is not expressed in our samples that show a very rapid decrease in the first portion of the trend. This idea of different grain sizes controlling the microstructure evolution and thus the frictional behavior of binary mixtures has been already suggested by *Niemeijer and Spiers* [2006] and *Moore and Lockner* [2011] for other types of binary mixtures. The overlapping grain size of talc and calcite thus facilitates the effective interconnection of talc lamellae even with small amounts of talc, i.e., 20%. The importance of the topology of the weakest mineral during deformation has been also suggested on the basis of previous experiments on intact cores of serpentinized peridotites [*Escartín et al.*, 2001]. In this study, serpentine coating olivine grain boundaries in the intact cores is interpreted as a key factor in controlling the nonlinear strength dependence on serpentinization. *Moore and Lockner* [2011] also performed velocity-stepping tests. In their experiments, at low talc content, the $(a - b)$ parameter approaches zero value, further suggesting that quartz framework exercises a strong control over the frictional behavior of quartz-rich mixtures. Adding talc, they observed an increase in $(a - b)$ in correspondence to the steeper portion of the friction degradation curve (Figure 11b). As observed also in other experimental studies on phyllosilicate-rich gouges [*den Hartog et al.*, 2014], an increase in the amount of quartz shifts the $(a - b)$ parameter toward more negative values, promoting velocity-weakening behavior. However, the velocity dependence does not increase monotonically with increasing phyllosilicate content. In quartz/talc mixtures [*Moore and Lockner*, 2011] the value of $(a - b)$ increases until a 50% talc content, the minimum amount of talc at which the localization of shear along talc-lined shears occurs. These

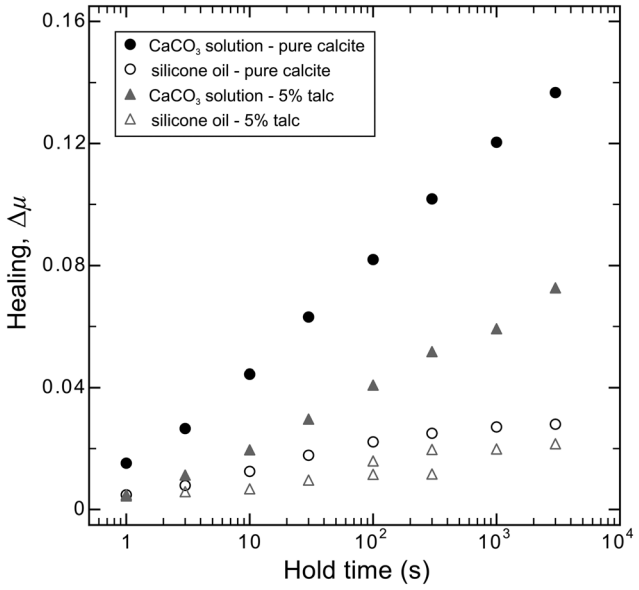

Figure 12. Comparison between frictional healing data from this study on 5% talc mixture and previous work on pure calcite [*Carpenter et al.*, 2013] resulting from experiments conducted with different pore fluids ($CaCO_3$-equilibrated water and silicone oil). All the plotted experiments are carried out at 5 MPa normal stress and 10 μm/s sliding velocity. The difference between the pure calcite samples at different saturation conditions suggests an important role of water-assisted processes, as solution and cementation, in enhancing the healing rate. The difference between the pure calcite and 5% talc sample in $CaCO_3$-water possibly results from the inhibition of calcite solution and cementation exerted by the presence of talc. The frictional healing of 5% talc sample in silicone oil is similar to that of pure calcite under the same saturation conditions.

results compare well with our velocity steps data that show the larger increase in $(a-b)$ in correspondence of the steeper portion of friction degradation that for calcite/talc mixture is achieved at 20% of talc (Figure 11a). We suggest a progressive stabilization of gouge, toward more positive $(a-b)$ values, with increasing talc content, as R_1 shears on talc alignments develop and increase in length, until a fully interconnected talc framework is reached. In addition, we noticed that, whereas at 5 MPa normal stress, the velocity dependence does not show a clear trend as a function of velocity, at 50 MPa $(a-b)$ values systematically decrease with increasing step velocity. From a theoretical point of view, the rate and state friction law states that a and b are constitutive properties of the material and independent of sliding velocity [e.g., *Dieterich*, 1979]; however our experiments, as well as previous studies, show that a velocity dependence of the a and b parameters exists [e.g., *Ikari et al.*, 2009a; *Niemeijer et al.*, 2010; *Ikari et al.*, 2011; *Moore and Lockner*, 2011; *Carpenter et al.*, 2014; *Verberne et al.*, 2014]. We suggest that in our experiments this rate dependence of $(a-b)$ can derive in part from a low-temperature plastic deformation of both talc lamellae [*Beeler et al.*, 2007] and calcite [e.g., *De Bresser et al.*, 2002; *Schubnel et al.*, 2006], being more efficient at higher normal stresses. On this basis, lower sliding velocity, at which plasticity is more efficient, correspond to higher $(a-b)$. Moreover, increasing normal stress (from 20 to 50 MPa) and increasing talc content (from 5 to 20%), we observe a switch toward negative values of b, resulting in a transition from a peak evolution of friction to a monotonic evolution of friction upon a velocity step. This behavior can be interpreted as the result of the interplay between brittle and plastic behaviors, possibly framed in a transition from a rate and state friction law, that can explain the peak evolution of pure calcite, to a flow law, that can explain the monotonic evolution of 20% talc gouge at high stress, as suggested from theoretical model by *Noda and Shimamoto* [2010] and *Shimamoto and Noda* [2014]. However, further investigation is required to discriminate the predominant deformation mechanism.

4.3. The Mechanisms of Frictional Healing

Frictional healing is a complex combination of different phenomena arising from the interplay of physical-mechanical and chemical processes occurring inside the gouge layer. Frictional strengthening of a granular gouge may result from porosity loss, due to mechanical and chemical compaction, and contact strengthening [e.g., *Scholz*, 2002]. At shallow-crustal conditions, compaction of binary mixtures of strong and weak minerals results from mechanical compaction, due to intergranular sliding, comminution, and clay particle plasticity, and chemical compaction, due to fluid-assisted processes such as pressure solution, cementation, and contact area growth [*Evans et al.*, 1999]. Under low-pressure and low-temperature conditions, mechanical compaction consists of a time-independent process that develops a locked aggregate [*Evans et al.*, 1999; *Zhang and Spiers*, 2005]. Contrarily, chemical compaction consists of a time-dependent creep [e.g., *Bos et al.*, 2000; *Bos and Spiers*, 2000, 2001]. Previous experiments on the healing of binary mixtures have been conducted on a mixture of kaolinite and halite [*Bos and Spiers*, 2000], which is in a first approximation, the basis

of comparison for mixtures of phyllosilicates and higher-strength minerals. Our results are consistent with their results that showed a decrease of ~1 order of magnitude in the healing rate with the addition of 25% kaolinite content in the halite gouge. Our slide-hold-slide experiments outline the key role played by talc in drastically reducing the restrengthening of the gouges. We suggest that talc strongly reduces fault healing by both mechanical processes via contact area saturation, and chemical processes via the inhibition of dissolution and cementation of calcite.

Our previous experiments on calcite gouges conducted with different saturation fluids [*Carpenter et al*., 2013] show different restrengthening behavior (Figure 12). Calcite samples were saturated both with brine and silicone oil, chosen due to the fact that it is an inert pore fluid inhibiting chemical processes. The healing of pure calcite sample in $CaCO_3$-equilibrated water solution increases linearly with the logarithm of hold time, a feature often observed in experiments conducted at room temperature and first described by *Dieterich* [1972]. Conversely, the healing of pure calcite in silicone oil is significantly lower and has a different trend with the logarithm of hold time: after an initial linear increase, healing stabilizes to a constant value, which appears to saturate at long hold times, possibly suggesting the maximum porosity reduction, due to only mechanical compaction of the layer, occurring via intergranular sliding. Thus, these experiments give insight into the contribution of mechanical compaction, in silicone oil-saturated condition, versus the contribution of chemical compaction, in brine-saturated condition in relation to frictional healing. Such contributions have been previously explored in experimental works on calcite deformed with different pore fluids [*Zhang and Spiers*, 2005; *Zhang et al*., 2010]. On the basis of these considerations, a possible mechanism able to explain the high frictional healing under brine-saturated conditions is a fluid-assisted intergranular cementation. The development of an interconnected network of cemented calcite grains leads to high healing values, consistent with the mechanism identified in previous works, such as the strengthening of welded contacts by hydrothermal reaction [*Tenthorey et al*., 2003; *Yasuhara et al*., 2005] and the gain in cohesion induced by grain cementation due to pressure solution [*Olsen et al*., 1998; *Bos et al*., 2000; *Kanagawa et al*., 2000; *Bos and Spiers*, 2002]. Another time-dependent compaction mechanism that we cannot rule out is water-assisted stress corrosion crack growth [*Yasuhara and Elsworth*, 2008]. Also, this process, the activation of which is essentially enhanced by the presence of pore water [*Atkinson and Meredith*, 1989], can be inhibited under silicone oil saturation. However, due to the abundance of fine-grained calcite in the starting material, stress corrosion crack growth is less favored. This mechanism is indeed more efficient with coarser grains, whereas cementation and pressure solution are more efficient with finer grains.

In contrast to the healing behavior of angular materials described above, in phyllosilicates, such as talc, the phyllosilicate foliation allows quick saturation of the contact area and thus no restrengthening [e.g., *Bos and Spiers*, 2000; *Niemeijer et al*., 2008; *Ikari et al*., 2009a; *Tesei et al*., 2012]. We suggest this mechanism as the main control for the almost zero healing value in our 20% talc experiments (Figures 3 and 6), in which, as shown by microstructures, deformation occurs along talc-rich planes incapable of increasing their contact area or strength.

Interestingly, our mechanical data show that adding a talc content of 5% to pure calcite results in a drop is the healing rate from $\beta \approx 0.0361$ to $\beta \approx 0.0196$. At the same time this value is still significantly higher with respect to the pure calcite value under silicone oil-saturated condition ($\beta \approx 0.0071$) (Figure 12). If the difference in the healing rate between calcite in $CaCO_3$-equilibrated water and calcite in silicone oil is due to calcite cementation or stress corrosion cracking along grains contacts, our result suggests an important role of talc in limiting such chemical process of calcite and reducing it by about 60%. In order to have more insights into the frictional healing of 5% talc gouges, we ran one additional experiment under silicone oil-saturated conditions. The healing of 5% talc with silicone oil (Figure 12) shows a trend similar to pure calcite under the same conditions, but with slightly lower values ($\beta \approx 0.0053$). These lower values may indicate a certain, even if minimal, mechanical effect of talc on gouge compaction. In these tests, talc is not pervasive enough throughout the gouge layer to strongly affect the mechanical behavior of pure calcite by preventing the contact of calcite grains, but at the same time, talc lamellae, even if present in a small quantity, do not contribute to the progressive mechanical compaction of calcite grains, thus limiting healing. Moreover, whereas in brine-saturated experiments, dilation and compaction data show a linearly increasing trend, in silicone oil saturation experiments they are characterized by lower values that saturate at long hold times (Figure S5), further supporting the idea of a water-assisted chemical process operating in the gouges.

In order to explain the 50% of reduction in healing properties of calcite induced by the addition of 5% talc, we suggest that the release of magnesium ions from talc into the pore water may play a key role. This process occurs at room temperature, as suggested by the increase in magnesium content of our saturating solution (see Table S1). Since it is known that magnesium ions in the pore fluid inhibits calcite precipitation [*Reddy and Wang*, 1980; *Davis et al*., 2000], we propose cementation as a plausible restrengthening mechanism in our calcite gouges and partial cementation inhibition due to magnesium ions as a plausible mechanism in our 5% talc gouge. The operation of such a mechanism is supported by recent experiments documenting the effect of fluid presence on the restrengthening of carbonate fault gouge [e.g., *Chen et al*., 2015] and the effect of fluid composition on calcite compaction [e.g., *Zhang and Spiers*, 2005] and demonstrating that magnesium ions slow pressure solution processes [e.g., *Zhang and Spiers*, 2005].

To summarize we show that 5% of talc within calcite-rich fault gouges reduces frictional healing of 50% and, since little to no healing can be explained by the physical role of 5% talc in saturating the contact areas of deformation zones, we suggest this is accomplished by the chemical role exerted by talc in hindering cementation processes.

5. Conclusion

We systematically investigated the frictional sliding behavior of calcite gouges containing different amounts of talc, performing a suite of 20 friction experiments conducted at room temperature, normal stresses up to 50 MPa, and saturated under different pore fluid, i.e., $CaCO_3$-equilibrated water and silicone oil, conditions. Our experiments highlight the role of even small amounts of talc in reducing the strength of natural faults and altering their mechanical behavior.

The shear strength of simulated calcite gouges is strongly affected by the presence of minor amounts of talc. The addition of 20% talc is responsible for a reduction of 70% in steady state friction, a marked increase in the velocity-strengthening behavior and a decrease in the amount of frictional healing to nearly zero. Microstructural observations show that 20% talc is the minimum amount of talc that allows the interconnection of talc lamellae throughout the entire sample, thus localizing deformation on talc-rich R_1 shear planes and substantially weakening the gouge. We propose that the change in the mechanical properties of talc/calcite mixture occurring by about 20% talc content results from a switch in the deformation mechanism from distributed cataclastic flow for pure calcite to localized sliding on talc-rich shear planes.

Amounts of talc that only partially affected the frictional strength are able to drastically influence the healing behavior at normal stress of 5 MPa. The rate of frictional healing of a synthetic calcite gouge is halved with the addition of only 5% talc (from $\beta \approx 0.0361$ to $\beta \approx 0.0196$). Moreover, under silicone oil saturated conditions the healing rate of 5% talc sample further decreases from $\beta \approx 0.0196$ to $\beta \approx 0.0053$, suggesting that some water-assisted restrengthening of the gouge happens in $CaCO_3$-equilibrated water experiments. We propose that the drop in healing, due to the addition of 5% talc, is related not only to the presence of talc between adjacent calcite grains that prevent contact area growth but also to the presence of talc-derived magnesium ions in water that inhibit calcite precipitation.

Our experimental data support the idea that talc-bearing mature fault zones in carbonates are mechanically weak, remain weak over geologic time periods, and fail via stable, aseismic creep, even if talc is present in limited amounts.

Acknowledgments
This research was carried out within the ERC Starting grant GLASS (259256). We thank Alexandre Schubnel, Andre Niemeijer, and one anonymous reviewer whose comments helped strengthen this manuscript. We also thank Telemaco Tesei, Giuseppe Di Stefano, Andrea Cavallo, and Daniele Cinti for fruitful discussions and assistance in the laboratory. Our data are available via FTP transfer upon request.

References

Atkinson, B. K., and P. G. Meredith (1989), The theory of sub-critical crack growth with application to minerals and rocks, in *Fracture Mechanics of Rocks*, edited by B. K. Atkinson, pp. 111–166, Academic, San Diego, Calif.

Bebout, G. E., and M. D. Barton (2002), Tectonic and metasomatic mixing in a high-T, subduction-zone mélange: Insights into the geochemical evolution of the slab-mantle interface, *Chem. Geol.*, *187*, 79–106, doi:10.1016/S0009-2541(02)00019-0.

Beeler, N. M., T. E. Tullis, A. K. Kronenberg, and L. A. Reinen (2007), The instantaneous rate dependence in low temperature laboratory rock friction and rock deformation experiments, *J. Geophys. Res.*, *112*, B07310, doi:10.1029/2005JB003772.

Bernoulli, D., and H. Weissert (1985), Sedimentary fabrics in Alpine ophicalcites South Pennine Arosa zone, Switzerland, *Geology*, *13*, 755–758, doi:10.1130/0091-7613(1985)13<755:SFIAOS>2.0.CO;2.

Billi, A. (2010), Microtectonics of low-P low-T carbonate fault rocks, *J. Struct. Geol.*, *32*, 1392–1402, doi:10.1016/j.jsg.2009.05.007.

Blanpied, M. L., C. J. Marone, D. A. Lockner, J. D. Byerlee, and D. P. King (1998), Quantitative measure of the variation in fault rheology due to fluid-rock interactions, *J. Geophys. Res.*, *103*, 9691–9712, doi:10.1029/98JB00162.

Bos, B., and C. J. Spiers (2000), Effect of phyllosilicates on fluid-assisted healing of gouge-bearing faults, *Earth Planet. Sci. Lett.*, *184*, 199–210, doi:10.1016/S0012-821X(00)00304-6.

Bos, B., and C. J. Spiers (2001), Experimental investigation into the microstructural and mechanical evolution of phyllosilicate-bearing fault rock under conditions favouring pressure solution, *J. Struct. Geol.*, *23*, 1187–1202, doi:10.1016/S0191-8141(00)00184-X.

Bos, B., and C. J. Spiers (2002), Fluid-assisted healing processes in gouge-bearing faults: Insights from experiments on a rock analogue system, *Pure Appl. Geophys.*, *159*, 2537–2566, doi:10.1007/s00024-002-8747-2.

Bos, B., C. J. Peach, and C. J. Spiers (2000), Slip behavior of simulated gouge-bearing faults under conditions favoring pressure solution, *J. Geophys. Res.*, *105*(B7), 16,699–16,717, doi:10.1029/2000JB900089.

Boschi, C., G. L. Früh-Green, and J. Escartín (2006), Occurrence and significance of serpentinite-hosted, talc- and amphibole-rich fault rocks in modern oceanic settings and ophiolite complexes: An overview, *Ofioliti*, *31*, 129–140.

Boutareaud, S., T. Hirose, M. Andréani, M. Pec, D.-G. Calugaru, A.-M. Boullier, and M.-L. Doan (2012), On the role of phyllosilicates on fault lubrication: Insight from micro- and nanostructural investigations on talc friction experiments, *J. Geophys. Res.*, *117*, B08408, doi:10.1029/2011JB009006.

Byerlee, J. D. (1978), Friction of rocks, *Pure Appl. Geophys.*, *116*, 615–626, doi:10.1007/BF00876528.

Carpenter, B. M., C. Marone, and D. M. Saffer (2011), Weakness of the San Andreas Fault revealed by samples from the active fault zone, *Nat. Geosci.*, *4*, 251–254, doi:10.1038/ngeo1089.

Carpenter, B. M., G. Di Stefano, C. Viti, and C. Collettini (2013), Relating mechanical behavior and microstructural observations in calcite fault gouge, paper presented at 2013, Fall Meeting, AGU, San Francisco, Calif., Abstract MR42A-03, 9–13 Dec.

Carpenter, B. M., M. M. Scuderi, C. Collettini, and C. Marone (2014), Frictional heterogeneities on carbonate-bearing normal faults: Insights from the Monte Maggio Fault, Italy, *J. Geophys. Res. Solid Earth*, *119*, 9062–9076, doi:10.1002/2014JB011337.

Chen, J., B. A. Verberne, and C. J. Spiers (2015), Interseismic re-strengthening and stabilization of carbonate faults by "non-Dieterich" healing under hydrothermal conditions, *Earth Planet. Sci. Lett.*, *423*, 1–12, doi:10.1016/j.epsl.2015.03.044.

Chester, F. M., and J. M. Logan (1987), Composite planar fabric of gouge from the Punchbowl Fault zone, California, *J. Struct. Geol.*, *9*, 621–634, doi:10.1016/0191-8141(87)90147-7.

Collettini, C., and R. E. Holdsworth (2004), Fault zone weakening and character of slip along low-angle normal faults: Insights from the Zuccale fault, Elba, Italy, *J. Geol. Soc.*, *161*, 1039–1051, doi:10.1144/0016-764903-179.

Collettini, C., and R. H. Sibson (2001), Normal faults normal friction?, *Geology*, *29*, 927–930, doi:10.1130/0091-7613(2001)029<0927:NFNF>2.0.CO;2.

Collettini, C., A. Niemeijer, C. Viti, and C. Marone (2009a), Fault zone fabric and fault zone weakness, *Nature*, *462*, 907–910, doi:10.1038/nature08585.

Collettini, C., C. Viti, S. A. F. Smith, and R. E. Holdsworth (2009b), Development of interconnected talc networks and weakening of continental low-angle normal faults, *Geology*, *37*(6), 567–570, doi:10.1130/G25645A.1.

Collettini, C., A. Niemeijer, C. Viti, S. A. F. Smith, and C. Marone (2011), Fault structure, frictional properties and mixed-mode fault slip behavior, *Earth Planet. Sci. Lett.*, *311*, 316–327, doi:10.1016/j.epsl.2011.09.020.

Collettini, C., G. Di Stefano, B. M. Carpenter, P. Scarlato, T. Tesei, S. Mollo, F. Trippetta, C. Marone, G. Romeo, and L. Chiaraluce (2014), A novel and versatile apparatus for brittle rock deformation, *Int. J. Rock Mech. Min.*, *66*, 114–123, doi:10.1016/j.ijrmms.2013.12.005.

Davis, K. J., P. M. Dove, and J. J. De Yoreo (2000), The role of Mg^{2+} as an impurity in calcite growth, *Science*, *290*(5494), 1134–1137, doi:10.1126/science.290.5494.1134.

de Bresser, J. H. P., B. Evans, and J. Renner (2002), On estimating the strength of calcite rocks under natural conditions, in *Deformation Mechanisms, Rheology and Tectonics: Current Status and Future Perspectives*, edited by S. de Meer et al., *Geol. Soc. London Spec. Publ.*, *200*, 309–329, doi:10.1144/GSL.SP.2001.200.01.18.

den Hartog, S. A. M., C. J. Peach, D. A. M. De Winter, C. J. Spiers, and T. Shimamoto (2012), Frictional properties of megathrust fault gouges at low sliding velocities: New data on effects of normal stress and temperature, *J. Struct. Geol.*, *38*, 156–171, doi:10.1016/j.jsg.2011.12.001.

den Hartog, S. A. M., D. M. Saffer, and C. J. Spiers (2014), The roles of quartz and water in controlling unstable slip in phyllosilicate-rich megathrust fault gouges, *Earth Planets Space*, *66*, 78, doi:10.1186/1880-5981-66-78.

Dieterich, J. H. (1972), Time-dependent friction in rocks, *J. Geophys. Res.*, *77*, 3690–3697, doi:10.1029/JB077i020p03690.

Dieterich, J. H. (1979), Modeling of rock friction: 1. Experimental results and constitutive equations, *J. Geophys. Res.*, *84*, 2161–2168, doi:10.1029/JB084iB05p02161.

Dieterich, J. H., and B. D. Kilgore (1994), Direct observation of frictional contacts: New insights for state-dependent properties, *Pure Appl. Geophys.*, *143*, 283–302, doi:10.1007/BF00874332.

d'Orazio, M., C. Boschi, and D. Brunelli (2004), Talc-rich hydrothermal rocks from the St. Paul and Conrad fracture zones in the Atlantic Ocean, *Eur. J. Mineral.*, *16*, 73–83, doi:10.1127/0935-1221/2004/0016-0073.

Escartín, J., G. Hirth, and B. Evans (2001), Strength of slightly serpentinized peridotites: Implications for the tectonics of oceanic lithosphere, *Geology*, *29*, 1023–1026, doi:10.1130/0091-7613(2001)029<1023:SOSSPI>2.0.CO;2.

Escartín, J., C. Mével, C. J. MacLeod, and A. M. McCaig (2003), Constrains on deformation conditions and the origin of oceanic detachments: The Mid-Atlantic Ridge core complex at 15°45'N, *Geochem. Geophys. Geosyst.*, *4*(8), 1067, doi:10.1029/2002GC000472.

Escartín, J., M. Andréani, G. Hirth, and B. Evans (2008), Relationship between the microstructural evolution and rheology of talc at elevated pressures and temperatures, *Earth Planet. Sci. Lett.*, *268*, 463–475, doi:10.1016/j.epsl.2008.02.004.

Evans, B., Y. Bernabé, and W. Zhu (1999), Evolution of pore structure and permeability of rocks in laboratory experiments, in *Growth, Dissolution and Pattern Formation in Geosystem*, edited by B. Jamteit and P. Meakin, pp. 327–344, Kluwer Acad. Publ., Dordrecht, Netherlands.

Fagereng, Å., and R. H. Sibson (2010), Melange rheology and seismic style, *Geology*, *38*, 751–754, doi:10.1130/G30868.1.

Faulkner, D. R., A. C. Lewis, and E. H. Rutter (2003), On the internal structure and mechanics of large strike-slip fault zones: Field observations of the Carboneras fault in southeastern Spain, *Tectonophysics*, *367*, 235–251, doi:10.1016/S0040-1951(03)00134-3.

Floyd, J. S., J. C. Mutter, A. M. Goodliffe, and B. Taylor (2001), Evidence for fault weakness and fluid flow within an active low-angle normal fault, *Nature*, *411*, 779–783, doi:10.1038/35081040.

Frye, K. M., and C. Marone (2002), Effect of humidity on granular friction at room temperature, *J. Geophys. Res.*, *107*(B11), 2309, doi:10.1029/2001JB000654.

Grasemann, B., and C. Tschegg (2012), Localization of deformation triggered by chemo-mechanical feedback processes, *Geol. Soc. Am. Bull.*, *124*, 737–745, doi:10.1130/B30504.1.

Hickman, S., and M. Zoback (2004), Stress orientations and magnitudes in the SAFOD pilot hole, *Geophys. Res. Lett.*, *31*, L15S12, doi:10.1029/2004GL020043.

Hirauchi, K.-I., S. A. M. den Hartog, and C. J. Spiers (2013), Weakening of the slab-mantle wedge interface induced by metasomatic growth of talc, *Geology*, *41*, 75–78, doi:10.1130/G33552.1.

Ikari, M. J., D. M. Saffer, and C. Marone (2009a), Frictional and hydrologic properties of clay-rich fault gouge, *J. Geophys. Res.*, *114*, B05409, doi:10.1029/2008JB006089.

Ikari, M. J., D. M. Saffer, and C. Marone (2009b), Frictional and hydrologic properties of a major splay fault system, Nankai subduction zone, *Geophys. Res. Lett.*, *36*, L20313, doi:10.1029/2009GL040009.

Ikari, M. J., C. Marone, and D. M. Saffer (2011), On the relation between fault strength and frictional stability, *Geology*, *39*, 83–86, doi:10.1130/G31416.1.

Jefferies, S. P., R. E. Holdsworth, C. A. J. Wibberley, T. Shimamoto, C. J. Spiers, A. R. Niemeijer, and G. E. Lloyd (2006), The nature and importance of phyllonite development in crustal-scale fault cores: An example from the Median Tectonic Line, Japan, *J. Struct. Geol.*, *28*, 220–235, doi:10.1016/j.jsg.2005.10.008.

Kanagawa, K., S. F. Cox, and S. Zhang (2000), Effects of dissolution-precipitation processes on the strength and mechanical behavior of quartz gouge at high-temperature hydrothermal conditions, *J. Geophys. Res.*, *105*(B5), 11,115–11,126, doi:10.1029/2000JB900038.

King, R. L., M. J. Kohn, and J. M. Eiler (2003), Constraints on the petrologic structure of the subduction slab-mantle interface from Franciscan Complex exotic ultramafic blocks, *Geol. Soc. Am. Bull.*, *115*, 1097–1109, doi:10.1130/B25255.1.

Kopf, A. (2001), Permeability variation across an active low-angle detachment fault, western Woodlark Basin (ODP Leg 180), and its implication for fault activation, in *The Nature and Tectonic Significance of Fault Zone Weakening*, edited by R. E. Holdsworth et al., *Geol. Soc. London Spec. Publ., 186*, 23–41, doi:10.1144/GSL.SP.2001.186.01.03.

Kopf, A., and K. M. Brown (2003), Friction experiments on saturated sediments and their implications for the stress state of the Nankai and Barbados subduction thrusts, *Mar. Geol.*, *202*, 193–210, doi:10.1016/s0025-3227(03)00286-x.

Lockner, D. A., C. Morrow, D. E. Moore, and S. Hickman (2011), Low strength of deep San Andreas fault gouge from SAFOD core, *Nature*, *472*, 82–85, doi:10.1038/Nature09927.

Logan, J. M., C. A. Dengo, N. G. Higgs, and Z. Z.. Wang (1992), Fabric of experimental fault zone: Their development and relationship to mechanical behavior, in *Fault Mechanics and Transport Properties of Rocks*, edited by B. Evans and T. Wong, pp. 33–67, Elsevier Academic, San Diego, Calif., doi:10.1016/S0074-6142(08)62814-4.

Lupini, J. F., A. E. Skinner, and P. R. Vaughan (1981), The drained residual strength of cohesive soils, *Geotechnique*, *31*, 181–213, doi:10.1680/geot.1981.31.2.181.

Mair, K., and C. Marone (1999), Friction of simulated fault gouge for a wide range of velocities and normal stresses, *J. Geophys. Res.*, *104*(B12), 28,899–28,914, doi:10.1029/1999JB900279.

Manning, C. E. (1995), Phase-equilibrium controls on SiO_2 metasomatism by aqueous fluid in subduction zones: Reaction at constant pressure and temperature, *Int. Geol. Rev.*, *37*, 1039–1073, doi:10.1080/00206819509465440.

Marone, C. (1998), Laboratory-derived friction laws and their application to seismic faulting, *Annu. Rev. Earth Planet. Sci.*, *26*, 643–696, doi:10.1146/annurev.earth.26.1.643.

Marone, C., and B. Kilgore (1993), Scaling of the critical slip distance for seismic faulting with shear strain in fault zones, *Nature*, *362*, 618–621, doi:10.1038/362618a0.

Marone, C., C. B. Raleigh, and C. H. Scholz (1990), Frictional behavior and constitutive modeling of simulated fault gouge, *J. Geophys. Res.*, *95*, 7007–7025, doi:10.1029/JB095iB05p07007.

Misra, S., S. Boutareaud, and J.-P. Burg (2014), Rheology of talc sheared at high pressure and temperature: A case study for hot subduction zones, *Tectonophysics*, *610*, 51–62, doi:10.1016/j.tecto.2013.10.009.

Moore, D. E., and D. A. Lockner (2004), Crystallographic controls on the frictional behavior of dry and water-saturated sheet structure minerals, *J. Geophys. Res.*, *109*, B03401, doi:10.1029/2003JB002582.

Moore, D. E., and D. A. Lockner (2008), Talc friction in the temperature range 25°–400°C: Relevance for fault-zone weakening, *Tectonophysics*, *449*, 120–132, doi:10.1016/j.tecto.2007.11.039.

Moore, D. E., and D. A. Lockner (2011), Frictional strengths of talc-serpentine and talc-quartz mixtures, *J. Geophys. Res.*, *116*, B01403, doi:10.1029/2010JB007881.

Moore, D. E., and M. Rymer (2007), Talc-bearing serpentines and creeping section of San Andreas fault, *Nature*, *448*, 795–797, doi:10.1038/nature06064.

Niemeijer, A. R., and C. J. Spiers (2005), Influence of phyllosilicates on fault strength in the brittle-ductile transition: Insights from rock analogue experiments, in *High-Strain Zones: Structure and Physical Properties*, edited by D. Bruhn and L. Burlini, *Geol. Soc. London Spec. Publ., 245*, 303–327, doi:10.1144/GSL.SP.2005.245.01.15.

Niemeijer, A. R., and C. J. Spiers (2006), Velocity dependence of strength and healing behavior in simulated phyllosilicate-bearing fault gouge, *Tectonophysics*, *427*, 231–253, doi:10.1016/j.tecto.2006.03.048.

Niemeijer, A., C. Marone, and D. Elsworth (2008), Healing of simulated fault gouges aided by pressure solution: Results from rock analogue experiments, *J. Geophys. Res.*, *113*, B04204, doi:10.1029/2007JB005376.

Niemeijer, A., C. Marone, and D. Elsworth (2010), Fabric induced weakness of tectonic faults, *Geophys. Res. Lett.*, *37*, L03304, doi:10.1029/2009GL041689.

Noda, H., and T. Shimamoto (2010), A rate- and state-dependent ductile flow law of polycrystalline halite under large shear strain and implications for transition to brittle deformation, *Geophys. Res. Lett.*, *37*, L09310, doi:10.1029/2010GL042512.

Numelin, T., C. Marone, and E. Kirby (2007), Frictional properties of natural fault gouge from a low-angle normal fault Panamint Valley, California, *Tectonics*, *26*, TC2004, doi:10.1029/2005TC001916.

Olsen, M., C. H. Scholz, and A. Léger (1998), Healing and sealing of a simulated fault gouge under hydrothermal conditions: Implications for fault healing, *J. Geophys. Res.*, *103*(B4), 7421–7430, doi:10.1029/97JB03402.

Peacock, S. M. (1987), Serpentinization and infiltration metasomatism in the Trinity peridotite, Klamath province, northern California: Implications for subduction zones, *Contrib. Mineral. Petrol.*, *95*, 55–70, doi:10.1007/BF00518030.

Reddy, M. M., and K. K. Wang (1980), Crystallization of calcium carbonate in the presence of metal ions: I. Inhibition of magnesium ion at pH 8.8 and 250°C, *J. Cryst. Growth*, *50*, 470–480, doi:10.1016/0022-0248(80)90095-0.

Reinen, L. A., and J. D. Weeks (1993), Determination of rock friction constitutive parameters using an iterative least squares inversion method, *J. Geophys. Res.*, *98*(B9), 15,937–15,950, doi:10.1029/93JB00780.

Richardson, E., and C. Marone (1999), Effects of normal stress vibrations on frictional healing, *J. Geophys. Res.*, *104*(B12), 28,859–28,878, doi:10.1029/1999JB900320.

Rimstidt, J. D. (1997), Quartz solubility at low temperatures, *Geochim. Cosmochim. Acta*, *61*, 2553–2558, doi:10.1016/S0016-7037(97)00103-8.

Roller, S., J. H. Behrmann, and A. Kopf (2001), Deformation fabrics of faulted rocks, and some syntectonics stress estimates from the active Woodlark Basin detachment zone, in *Non-Volcanic Rifting of Continental Margins: A Comparison of Evidence From Land and Sea*, edited by R. C. L. Wilson et al., *Geol. Soc. London Spec. Publ., 187*, 319–334, doi:10.1144/GSL.SP.2001.187.01.16.

Ruina, A. (1983), Slip instability and state variable friction laws, *J. Geophys. Res.*, *88*, 10,359–10,370, doi:10.1029/JB088iB12p10359.
Saffer, D., K. Frye, C. Marone, and K. Mair (2001), Laboratory results indicating complex and potentially unstable frictional behavior of smectite clay, *Geophys. Res. Lett.*, *28*, 2297–2300, doi:10.1029/2001GL012869.
Saffer, D. M., and C. Marone (2003), Comparison of smectite- and illite-rich gouge frictional properties: Application to the updip limit of the seismogenic zone along subduction megathrusts, *Earth Planet. Sci. Lett.*, *215*, 219–235, doi:10.1016/S0012-821X(03)00424-2.
Sammis, C. G., and S. J. Steacy (1994), The micromechanics of friction in a granular layer, *Pure Appl. Geophys.*, *142*, 777–794.
Schleicher, A. M., B. A. van der Pluijm, and L. N. Warr (2010), Nanocoatings of clay and creep of the San Andreas fault at Parkfield California, *Geology*, *38*, 667–670, doi:10.1130/G31091.1.
Scholz, C. H. (1998), Earthquakes and friction laws, *Nature*, *391*, 37–42, doi:10.1038/34097.
Scholz, C. H. (2002), *The Mechanics of Earthquakes and Faulting*, Cambridge Univ. Press, Cambridge, U. K.
Schroeder, T., and B. E. John (2004), Strain localization on an oceanic detachment fault system, Atlantis Massif, 30°N, Mid-Atlantic Ridge, *Geochem. Geophys. Geosyst.*, *5*, Q11007, doi:10.1029/2004GC000728.
Schubnel, A., E. Walker, B. D. Thompson, J. Fortin, Y. Guéguen, and R. P. Young (2006), Transient creep, aseismic damage and slow failure in Carrara marble deformed across the brittle-ductile transition, *Geophys. Res. Lett.*, *33*, L17301, doi:10.1029/2006GL026619.
Scuderi, M. M., A. R. Niemeijer, C. Collettini, and C. Marone (2013), Frictional properties and slip stability of active faults within carbonate-evaporite sequences: The role of dolomite and anhydrite, *Earth Planet. Sci. Lett.*, *369*, 220–232, doi:10.1016/j.epsl.2013.03.24.
Shimamoto, T., and H. Noda (2014), A friction to flow constitutive law and its application to a 2-D modeling of earthquakes, *J. Geophys. Res. Solid Earth*, *119*, 8089–8106, doi:10.1002/2014JB011170.
Taylor, B., and P. Huchon (2002), Active continental extension in the western Woodlark Basin: A synthesis of Leg 180 results, *Proc. Ocean Drill. Program Sci. Results*, *180*, 1–36.
Tembe, S., D. A. Lockner, and T. -F. Wong (2010), Effect of clay content and mineralogy on frictional sliding behavior of simulated gouges: Binary and ternary mixtures of quartz, illite, and montmorillonite, *J. Geophys. Res.*, *115*, B03416, doi:10.1029/2009JB006383.
Tenthorey, E., S. F. Cox, and H. F. Todd (2003), Evolution of strength recovery and permeability during fluid-rock reaction in experimental fault zones, *Earth Planet. Sci. Lett.*, *206*(1–2), 161–172, doi:10.1016/S0012-821X(02)01082-8.
Tesei, T., C. Collettini, B. M. Carpenter, C. Viti, and C. Marone (2012), Frictional strength and healing behavior of phyllosilicate-rich faults, *J. Geophys. Res.*, *117*, B09402, doi:10.1029/2012JB009204.
Tesei, T., C. Collettini, M. R. Barchi, B. M. Carpenter, and G. Di Stefano (2014), Heterogeneous strength and fault zone complexity of carbonate-bearing thrusts with possible implications for seismicity, *Earth Planet. Sci. Lett.*, *408*, 307–318, doi:10.1016/j.epsl.2014.10.021.
Townend, J., and M. D. Zoback (2000), How faulting keeps the crust strong, *Geology*, *28*, 399–402, doi:10.1130/0091-7613(2000)28<399:HFKTCS>2.0.CO;2.
Verberne, B. A., C. J. Spiers, A. R. Niemeijer, J. H. De Bresser, D. A. M. De Winter, and O. Plümper (2014), Frictional properties and microstructure of calcite-rich fault gouges sheared at sub-seismic sliding velocities, *Pure Appl. Geophys.*, *171*, 2617–2640, doi:10.1007/s00024-013-0760-0.
Viti, C., and C. Collettini (2009), Growth and deformation mechanisms of talc along a natural fault: A micro/nanostructural investigation, *Contrib. Mineral. Petrol.*, *158*, 529–542, doi:10.1007/s00410-009-0395-4.
Vrolijk, P., and B. A. van der Pluijm (1999), Clay gouge, *J. Struct. Geol.*, *21*, 1039–1048, doi:10.1016/S0191-8141(99)00103-0.
Weeks, J. D., and T. E. Tullis (1985), Frictional sliding of dolomite: A variation in constitutive behavior, *J. Geophys. Res.*, *90*, 7821–7826, doi:10.1029/JB090iB09p07821.
Wintsch, R. P., R. Christoffersen, and A. K. Kronenberg (1995), Fluid-rock reaction weakening of fault zones, *J. Geophys. Res.*, *100*, 13,021–13,032, doi:10.1029/94JB02622.
Yasuhara, H., and D. Elsworth (2008), Compaction of a rock fracture moderated by competing roles of stress corrosion and pressure solution, *Pure Appl. Geophys.*, *165*, 1289–1306, doi:10.1007/s00024-008-0356-2.
Yasuhara, H., C. Marone, and D. Elsworth (2005), Fault zone restrengthening and frictional healing: The role of pressure solution, *J. Geophys. Res.*, *110*, B06310, doi:10.1029/2004JB00327.
Zhang, X., and C. J. Spiers (2005), Compaction of granular calcite by pressure solution at room temperature and effects of pore fluid chemistry, *Int. J. Rock Mech. Min. Sci.*, *42*(7–8), 950–960, doi:10.1016/j.ijrmms.2005.05.017.
Zhang, X., C. J. Spiers, and C. J. Peach (2010), Compaction creep of wet granular calcite by pressure solution at 28°C to 150°C, *J. Geophys. Res.*, *115*, B09217, doi:10.1029/2008JB005853.